The Plant Cell, Vol. 29: 1388–1405, June 2017, www.plantcell.org

SH3 Domain-Containing Protein 2 Plays a Crucial Role at the Step of Membrane Tubulation during Cell Plate Formation

Gyeongik Ahn,[a] Hyeran Kim,[a,1] Dae Heon Kim,[a,2] Hong Hanh,[b] Youngdae Yoon,[c,3] Indira Singaram,[c] Kaveesha J. Wijesinghe,[d] Kristen A. Johnson,[d] Xiaohong Zhuang,[e] Zizhen Liang,[e] Robert V. Stahelin,[d,f] Liwen Jiang,[e] Wonhwa Cho,[c] Byung-Ho Kang,[e] and Inhwan Hwang[a,b,4]

[a] Department of Life Sciences, Pohang University of Science and Technology, Pohang 790-784, Korea
[b] Division of Integrative Biosciences and Biotechnology, Pohang University of Science and Technology, Pohang 790-784, Korea
[c] Department of Chemistry, University of Illinois at Chicago, Chicago, Illinois 60607
[d] Department of Chemistry and Biochemistry, University of Notre Dame, Notre Dame, Indiana 46556
[e] School of Life Sciences, Chinese University of Hong Kong, Shatin, New Territories, Hong Kong 999077, China
[f] Department of Biochemistry and Molecular Biology, Indiana University School of Medicine-South Bend, South Bend, Indiana 46617

ORCID IDs: 0000-0002-2480-8210 (X.Z.); 0000-0002-1388-1367 (I.H.)

During cytokinesis in plants, *trans*-Golgi network-derived vesicles accumulate at the center of dividing cells and undergo various structural changes to give rise to the planar cell plate. However, how this conversion occurs at the molecular level remains elusive. In this study, we report that SH3 Domain-Containing Protein 2 (SH3P2) in *Arabidopsis thaliana* plays a crucial role in converting vesicles to the planar cell plate. *SH3P2* RNAi plants showed cytokinesis-defective phenotypes and produced aggregations of vesicles at the leading edge of the cell plate. SH3P2 localized to the leading edge of the cell plate, particularly the constricted or curved regions of the cell plate. The BAR domain of SH3P2 induced tubulation of vesicles. SH3P2 formed a complex with dynamin-related protein 1A (DRP1A) and affected DRP1A accumulation to the cell plate. Based on these results, we propose that SH3P2 functions together with DRP1A to convert the fused vesicles to tubular structures during cytokinesis.

INTRODUCTION

All living organisms undergo cell division to increase the number of cells. At the end of cell division, the parental cells separate into two daughter cells. The final process of cell division is called cytokinesis. Thus, cytokinesis is the process of partitioning the cytoplasm of a dividing cell to form two daughter cells. The mechanism of cytokinesis in plants is very different from that in non-plant organisms. In plant cells, a plant-specific compartment called the cell plate is generated at the center of the dividing cell (Samuels et al., 1995; Verma, 2001; Jürgens, 2005). The entire process of cell plate formation has been defined in detail at the electron microscopy (EM) level (Otegui et al., 2001; Seguí-Simarro et al., 2004). Cell plate formation starts with the accumulation of vesicles largely derived from the *trans*-Golgi network (TGN) at the center of the dividing cell. These vesicles are homotypically fused to form hourglass-shaped vesicle intermediates, which are the building blocks of the tubulo-vesicular network (TVN) (Otegui et al., 2001; Seguí-Simarro et al., 2004; Lukowitz et al., 1996; Chow et al., 2008). The lumen of the TVN is filled with cell wall polysaccharides, especially callose. The TVN is converted into a stronger and more stable tubular network (Thiele et al., 2009; Miart et al., 2014). This matures to the planar fenestrated sheet (PFS) and finally to a new cell wall. Repetitions of these processes at the leading edge of the cell plate allow the cell plate to expand centrifugally toward the parent cell wall from the center of the dividing cell (Otegui et al., 2001; Seguí-Simarro et al., 2004; Lukowitz et al., 1996).

Numerous proteins are required for membrane structure remodeling in cell plate formation. In this process, the first step is homotypic fusion of incoming vesicles, which is mediated by two distinct types of cytokinesis-specific Qa-SNARE KNOLLE-containing complexes: One of them is composed of KNOLLE, SNAP33, and VAMP721,722 (Qa, Qb,c, and R), and the other is composed of KNOLLE, NPSN11, SYP71, and VAMP721,722 (Qa, Qb, Qc, and R) (El Kasmi et al., 2013). The Sec1/Munc18 protein KEULE also plays a critical role in cell plate formation by promoting *trans*-SNARE complex formation via interaction of the fusion-competent open form of KNOLLE (Park et al., 2012). After vesicle fusion, the process of membrane remodeling is crucial to produce strong building blocks of the cell plate and to maintain the stable structure. Dynamin-like molecules, which polymerize to produce a ring-like structure, are involved in tubulation of hourglass-shaped vesicle intermediates to produce dumbbell-shaped membrane structures and also to generate the TVN (Otegui et al., 2001; Seguí-Simarro et al., 2004). However, except for dynamin-like proteins, the other proteins involved in membrane remodeling

[1] Current address: Center for Genome Engineering, Institute for Basic Science, Daejeon 34047, Korea.
[2] Current address: Department of Biology, Sunchon National University, Sunchon 57922, Republic of Korea.
[3] Current address: Department of Environmental Health Science, Konkuk University, Seoul 143-701, Korea.
[4] Address correspondence to ihhwang@postech.ac.kr.
The author responsible for distribution of materials integral to the findings presented in this article in accordance with the policy described in the Instructions for Authors (www.plantcell.org) is: Inhwan Hwang (ihhwang@postech.ac.kr).
www.plantcell.org/cgi/doi/10.1105/tpc.17.00108

during cell plate formation are not known. In addition, the exact mechanism by which tubulation occurs remains elusive.

The *Arabidopsis thaliana* genome contains 16 dynamin-related proteins (DRPs) grouped into six functional subfamilies (DRP1–6) on the basis of the phylogeny and functional domains of the proteins (Hong et al., 2003). Among them, members of the DRP1 and DRP2 subfamilies and DRP5A are involved in cytokinesis (Kang et al., 2003; Collings et al., 2008; Fujimoto et al., 2008; Miyagishima et al., 2008). Although DRP1A polymerizes into dynamin-like rings at membrane tubules during cell plate formation (Otegui et al., 2001; Zhang et al., 2000), DRP1A polymers do not induce liposome tubulation in vitro (Backues and Bednarek, 2010). These results raise the possibility that additional protein factors are necessary for DRP1A-mediated tubulation during cell plate formation. In animals, endophilin, which contains BAR (Bin/Amphiphysin/Rvs) and SH3 (src homology-3) domains, recruits dynamins and promotes fission of clathrin-coated vesicles (Sundborger et al., 2011). In vitro studies showed the relationship between endophilin and dynamin-2 (Dyn2); membrane curvature induced by the BAR domain of endophilin facilitates Dyn2-catalyzed vesicle release. On the other hand, the interaction between the SH3 domain of endophilin and the PRD (proline/arginine-rich domain) of Dyn2 inhibits scaffolding activity (Neumann and Schmid, 2013). Therefore, BAR and SH3 domain-containing proteins regulate the activity of dynamins in an opposite manner.

In Arabidopsis, three SH3 domain-containing proteins (SH3Ps), SH3P1, SH3P2, and SH3P3, have been identified. In addition, they all contain an N-terminal BAR domain (Lam et al., 2001; Zhuang et al., 2013). SH3P1 and SH3P3 are involved in trafficking of clathrin-coated vesicles (Lam et al., 2001, 2002). SH3P2 is involved in autophagosome formation and vacuole trafficking (Zhuang et al., 2013; Gao et al., 2014; Kolb et al., 2015), as well as crosstalk between the endocytic and autophagic pathways (Gao et al., 2015; Zhuang et al., 2015). These studies showed the role of SH3Ps in nondividing cells.

In this study, we further investigated the physiological role of Arabidopsis SH3Ps and provide evidence that SH3P2 plays a crucial role in cell plate formation via tubulation of membrane structures and is required for DRP1A localization to the cell plate during cytokinesis.

RESULTS

Loss-of-Function Mutation or RNAi-Mediated Suppression of *SH3P2* Causes a Defect in Germination or Plant Growth

To gain insight into the physiological role of the SH3Ps in Arabidopsis (i.e., SH3P1, SH3P2, and SH3P3), we identified the T-DNA insertion mutants, *sh3p1*, *sh3p2*, and *sh3p3*, respectively. The *sh3p1* and *sh3p2* mutants had the T-DNA in the last intron, and the *sh3p3* mutant had the T-DNA in the fifth exon (Supplemental Figures 1A and 1B). The absence of full-length transcripts in these mutants was confirmed by RT-PCR (Supplemental Figure 1C). Neither *sh3p1* nor *sh3p3* mutant plants showed a noticeable aberrant phenotype. Only *sh3p2* mutant plants showed delayed germination, but almost normal growth after germination (Supplemental Figures 1E and 1F). To test for any functional redundancy, we generated double and triple mutants of *sh3p1*, *sh3p2*, and *sh3p3*. Of these double mutants, only those with *sh3p2* showed a slight delay in germination. In addition, triple mutants also showed slightly delayed germination. However, the degree of delay in germination was more severe in the *sh3p2* single mutant than in the double or triple mutants with the *sh3p2* mutation, indicating that SH3P2 does not have any functional redundancy with SH3P1 and SH3P3 in germination.

These loss-of-function mutants did not show any visible phenotype, except for the delayed germination phenotype of *sh3p2* mutant plants. *sh3p1* and *sh3p2* plants had a T-DNA insertion in the last intron. SH3P2 protein levels were reduced in the *sh3p2* mutant ~30% (Supplemental Figure 1D). Moreover, it is possible that these mutant plants still produce a truncated form of proteins that have only a minor defect in their function (Supplemental Figure 1C). Recently, Zhuang et al. (2013) generated transgenic plants harboring an *SH3P2* RNAi construct under the control of the dexamethasone (DEX)-inducible promoter (*SH3P2* RNAi plants). Thus, to get a better idea about the physiological role of SH3P2, we examined the phenotype of *SH3P2* RNAi plants and found that DEX-treated *SH3P2* RNAi plants displayed severe growth defects. To define the exact nature of the defect, we closely examined the root tissues and found that the root cell files starting from the quiescent center showed irregular patterns and contained cells with incomplete cell walls (Figures 1A to 1C).

The *SH3P2* RNAi plant phenotype raises the possibility that these plants have a defect in cell plate formation. We monitored cell plate formation in DEX-treated *SH3P2* RNAi plants using FM4-64 in a time-dependent manner. FM4-64, a lipophilic dye, is used as a tracer of endocytosis and also stains the cell plate (Bolte et al., 2004). In control plants with no DEX treatment, FM4-64 accumulated at the cell plate located at the center of dividing root cells and the FM4-64-stained structure elongated toward the lateral plasma membranes with time, as reported previously (Song et al., 2012). In DEX-treated *SH3P2* RNAi plants, FM4-64 also accumulated at the cell plate, but the FM4-64-stained structure showed much slower growth with time and had a blurry boundary compared with that in control plants. Moreover, the elongation direction was not perpendicular to the lateral plasma membrane but bended downward. Eventually, cell plate growth was halted and cell wall stubs were generated (Figure 1D), indicating that DEX-treated *SH3P2* RNAi plants have a defect in cell plate formation. We obtained Z-stack images of the leading edge of the cell plate from control or DEX-treated *SH3P2* RNAi plants. The leading edge of the cell plate produced a sharp band in control plants, but a bulky structure with a blurry boundary in DEX-treated *SH3P2* RNAi plants (Figure 1E). In addition, the intensity of FM4-64 staining was abruptly altered at time points between 20 and 25 min (Figure 1D), suggesting that SH3P2 plays a crucial role at the maturation region, as well as at the leading edge of the cell plate.

SH3P2 Localizes to the Cell Plate and Is Involved in Various Stages of Cell Plate Formation

To gain insight into the physiological role of SH3P2 in cell plate formation, we examined the localization of SH3P2. We generated transgenic plants expressing YFP-tagged *SH3P2* under the control of the native promoter. In previous studies, SH3P2-sGFP

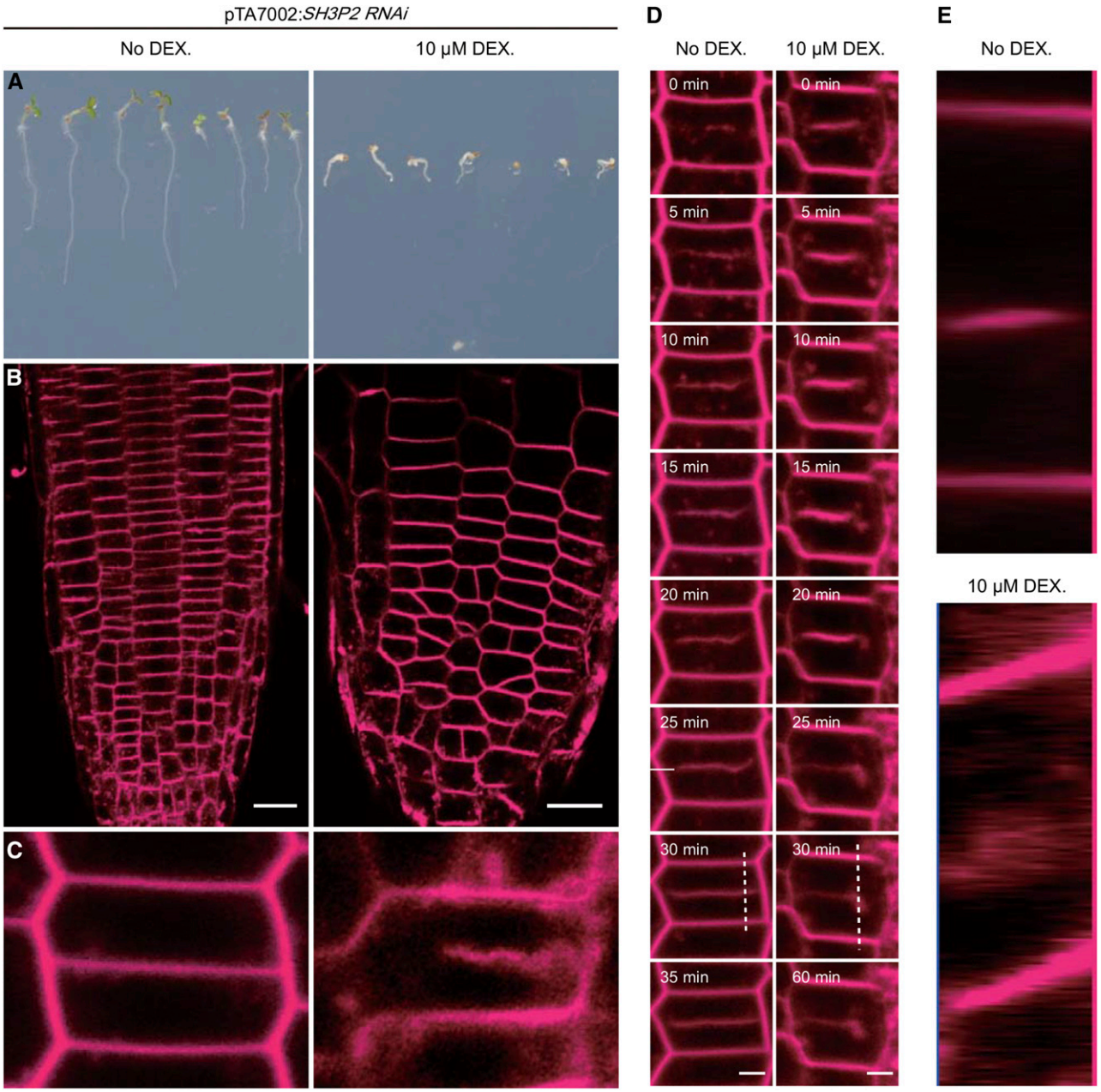

Figure 1. *SH3P2* RNAi Plants Display a Defect in Cell Plate Formation.

(A) to **(E)** Phenotypes of *SH3P2* RNAi plants. Plants were grown on 0.5× MS plates with or without DEX (10 μM) for 5 d. Overall growth pattern **(A)**, abnormally divided root cells **(B)**, and cell wall stubs **(C)**. Bar = 20 μm.
(D) Cell plate formation was monitored in root cells at the fixed focal plane at the indicated time points in the presence and absence of 10 μM DEX. Bar = 5 μm.
(E) A 3D image of the cell plate. Serial sections of images of the cell plate indicated by the white dotted line in **(D)** were used to construct a 3D image.
(B) to **(E)** Magenta fluorescent signals were generated by FM4-64 staining.

localized to the plasma membrane, autophagosomes, and vesicles; clathrin light chain (CLC)-positive membrane compartments (69.0%), early endosome/TGN (16.0%), and late endosome/multivesicular body (7.2%) (Zhuang et al., 2013; Kolb et al., 2015). Consistent with the previous results, SH3P2-YFP localized to the plasma membrane and endosomal compartments in nondividing cells of root tissues (Figure 2B). In addition, SH3P2-YFP localized to the cell plate in dividing cells of root tissues (Figure 2A), consistent with the notion that SH3P2 plays a role in cell plate formation in dividing cells. To further test its possible involvement in cell plate formation, we closely monitored the spatial and temporal localization pattern of SH3P2-GFP during cytokinesis after

staining with FM4-64. SH3P2-GFP colocalized with FM4-64 to the central cell plate at early time points (0–5 min). At later time points (15–45 min), SH3P2 showed a differential accumulation pattern with FM4-64, namely, higher levels at both leading edges, but weakly at the central region of the cell plate. By contrast, FM4-64 accumulated to higher levels at the center of the cell plate and to lower levels at both leading edges (Figure 2C). Consistent with these images, SH3P2-GFP produced ring-like structures at both leading edges in the 3D projection image at the 25 min time point (Figure 2D), indicating that SH3P2 plays a role in the growing region of the cell plate.

Many proteins localize to the cell plate but give different temporal and spatial localization patterns depending on their function in cell plate formation (Park et al., 2014). So, we compared the localization pattern of SH3P2 with that of other proteins, i.e., KNOLLE, DRP1A, and CLC, to investigate the role of SH3P2 at the cell plate. KNOLLE, the cytokinesis-specific Qa-SNARE, is involved in fusion of incoming vesicles at the growing region of the cell plate (Lukowitz et al., 1996). We analyzed these proteins for their colocalization. SH3P2-sGFP closely overlapped with KNOLLE at the cell plate. The linear Pearson correlation coefficient (r_p) and the nonlinear Spearman's rank correlation coefficient (r_s) of SH3P2-sGFP and KNOLLE were 0.831 and 0.840, respectively, confirming the close overlap (Supplemental Figures 2A and 2D). Next, we compared it with DRP1A, which is involved in membrane tubulation at the growing region of the cell plate (Otegui et al., 2001; Kang et al., 2003; Fujimoto et al., 2008). SH3P2-sGFP also showed a high degree of overlap with DRP1A at the leading edges (r_p = 0.530 and r_s = 0.606), but SH3P2-sGFP signals were much stronger than DRP1A signals in the region internal to the growing edges (Supplemental Figures 2B and 2E). This is similar to the relationship in the localization pattern between KNOLLE and DRP1A. KNOLLE stays longer at the cell plate than does DRP1C (Park et al., 2014). CLC, the small subunit of clathrin, is another protein that localizes to the cell plate and plays a role in trafficking from the cell plate at the maturation stage during cell plate formation (Song et al., 2012). SH3P2-sGFP highly overlapped with CLC (r_p = 0.818 and r_s = 0.836) (Supplemental Figures 2C and 2F). However, SH3P2-sGFP colocalized with CLC in the central region of the cell plate, but not the growing edges. These results suggest that SH3P2 functions at the growing region of the cell plate in the early as well as late stages of cell plate formation.

Cell plate formation involves a series of processes that convert vesicles to the planar membrane structure through various structural changes (Samuels et al., 1995; Otegui et al., 2001; Seguí-Simarro et al., 2004). Thus, one of the key steps is the tubulation of vesicular membrane structures. Many proteins have been identified that can induce tubulation of vesicular structures in various cellular processes such as endosomal trafficking and endocytosis (Zimmerberg and Kozlov, 2006). These include dynamins and BAR domain-containing proteins (Neumann and Schmid, 2013; Ferguson et al., 2009; Mim et al., 2012). Indeed, DRP1A, a member of the dynamin family, is proposed to play a role in tubular structure formation at the leading edge of the cell plate via constriction of membranes (Otegui et al., 2001; Kang et al., 2003; Collings et al., 2008; Fujimoto et al., 2008). To gain further insight into the relationship between SH3P2 and DRP1A in cell plate formation, we compared the localization of SH3P2 with that of DRP1A in detail (Figure 3). Serial optical Z-section images were obtained at 1-μm intervals to observe colocalization in various stages of cell plate formation. SH3P2-sGFP and DRP1A-mRFP showed both close overlapping and distinct localization patterns, which were identical to colocalization patterns of SH3P2-sGFP and endogenous DRP1A detected with DRP1A antibody (Supplemental Figure 2B). At the rim of the cell plate, both proteins showed a higher degree of colocalization, whereas at the more central regions of the cell plate, the signal intensity of SH3P2-sGFP was stronger than that of DRP1A (Figures 3E to 3H). Thus, SH3P2 locates on the cell plate more broadly than does DRP1A. Overall, r_p and r_s of SH3P2-sGFP and DRP1A-mRFP ranged from 0.575 to 0.858 and from 0.594 to 0.858, respectively.

SH3P2 Localizes to the Constricted or Curved Region of Membranes at the Growing Region of the Cell Plate

Multiple sequence alignment using Clustal revealed that SH3P2 has an N-terminal coiled-coil region with homology to the BAR domain, which has the ability to induce tubular structures from lipid vesicles (Takei et al., 1999; Peter et al., 2004; Frost et al., 2008). To confirm whether the N-terminal coiled-coil region of SH3P2 has BAR domain features, we first examined whether the SH3P2 BAR domain has structural features for lipid binding by comparing it with known BAR domains. BAR domains bind to the negatively charged membrane surface and induce membrane deformation using their intrinsic curvatures (Peter et al., 2004). The positively charged residues on their concave surface play a key role in the interaction with the negatively charged membrane surface. Homology modeling by Modeler using the endophilin A1 BAR domain as a template suggested the presence of basic patches, including R155, R160, R172, R173, and K189, on the concave surface of the SH3P2 BAR domain (Supplemental Figures 3A and 3B). This result prompted us to experimentally examine the lipid binding of the SH3P2 BAR domain. In addition, to determine if these basic residues are involved in membrane binding of the SH3P2 BAR domain, we measured the effect of mutating them to glutamic acid in different combinations on membrane binding of the domain. The wild type and mutants of the SH3P2 BAR domain were expressed as His-tagged forms in *Escherichia coli*.

We first determined the lipid binding affinity and specificity of the wild-type SH3P2 BAR domain by surface plasmon resonance (SPR) analysis using vesicles containing various phosphoinositides (PtdInsPs). The SH3P2 BAR domain showed the highest response to vesicles containing PtdIns(3,4,5)P_3, followed by those containing PtdIns(4,5)P_2 and PtdIns(3,4)P_2 (Figure 4A). It showed minimal binding to phosphatidylinositol monophosphates, including PtdIns(3)P. Equilibrium SPR analysis showed that the SH3P2 BAR domain bound to 1-palmitoyl-2-oleoyl-sn-glycero-3-phosphocholine (POPC)/1-palmitoyl-2-oleoyl-sn-glycero-3-phosphoserine (POPS)/PtdIns(3,4,5)P_3 (77:20:3) vesicles with $K_d = 30 \pm 2$ nM (Figures 4C and 4D). PtdIns(3,4,5)P_3 selectivity of the AtSH3P2 BAR domain and its affinity for POPC/POPS/PtdIns(3,4,5)P_3 (77:20:3) vesicles are similar to those of the endophilin A1 BAR domain (Yoon et al., 2012). Mutational analysis showed that basic residues in the concave surface of the SH3P2 BAR domain play important roles in its membrane binding. The

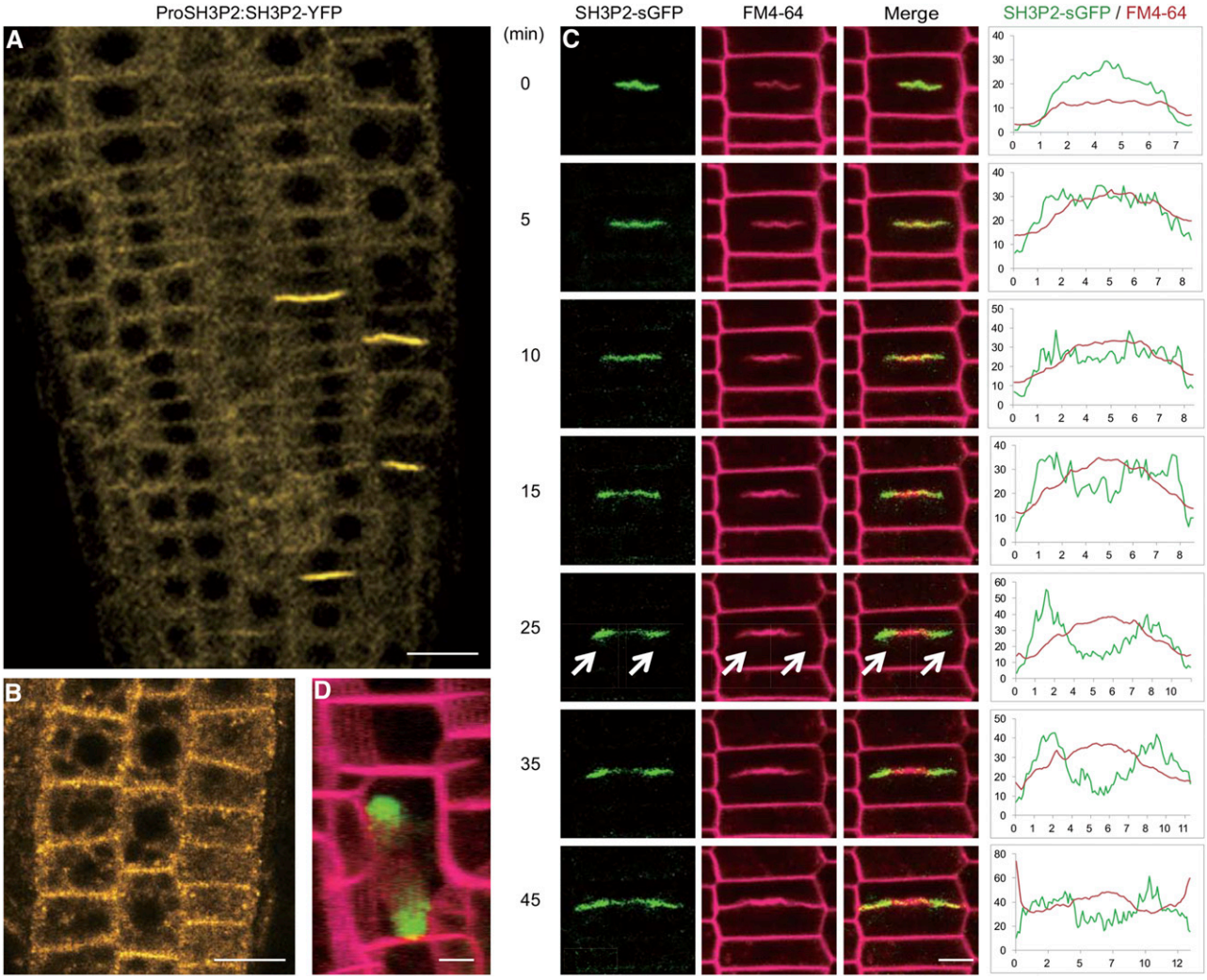

Figure 2. SH3P2 Localizes to the Plasma Membrane, Endosomes, and Cell Plate in the Growing Region of Roots.

(A) and **(B)** Localization of SH3P2-YFP expressed under the control of the native promoter was examined in whole root tissues **(A)** or single cells **(B)**. Bar = 20 μm.

(C) Localization of SH3P2-GFP to the cell plate. The localization of SH3P2-GFP expressed under the control of the CaMV 35S promoter together with FM4-64 was monitored at the indicated time points during cell plate formation. Arrows indicate the leading edges of the growing cell plate. In graphs, the *y* axis shows the fluorescence intensity of SH3P2-sGFP (Green) and FM4-64 (Magenta) at the cell plate and the *x* axis is distance (μm). Bar = 5 μm.

(D) A 3D image reconstructed using serial sections at the 25 min time point shown in **(C)**. The reconstruction only includes part but not the whole cell plate. Bar = 5 μm.

mutants R160/R161E (B mutant) and K189E (D mutant) showed significantly reduced binding to PtdIns(3,4,5)P_3-containing vesicles, whereas the multisite mutants Q154/R155/R160/R161E (AB mutant) and Q154/R155/R160/Q161/R172/R173/K189E (ABCD mutant) showed no binding (Figure 4B).

To assess if the SH3P2 BAR domain was able to induce changes to liposome morphology, we investigated liposome structural changes using transmission electron microscopy. Liposomes containing either POPC:POPE:PI(3,4,5)P_3 or POPC:POPE:PI(4,5)P_2 were imaged with and without incubation of the SH3P2 BAR domain or respective mutations (Figures 4E to 4L). After 20 min of incubation of PI(3,4,5)P3 with the SH3P2 BAR domain, extensive tubulation of liposomes was observed (Figure 4F). Quantification of tubules per liposome (Figure 4L) revealed an average tubule per liposome number of 2.4. By contrast, incubation of several of the SH3P2 BAR domain mutations with PI(3,4,5)P_3 containing liposomes lead to a significant reduction in the number of tubules per liposome. The D, AB, and ABCD mutations all lead to a statistically significant reduction in tubulation, and the AB and ABCD mutations in particular had little detectable evidence of liposome tubulation. The B mutant led to a lower average number of tubules per liposome, but this result was not statistically significant. To determine if the SH3P2 BAR domain was sufficient to induce tubulation to liposomes containing PI(4,5)P_2, which may

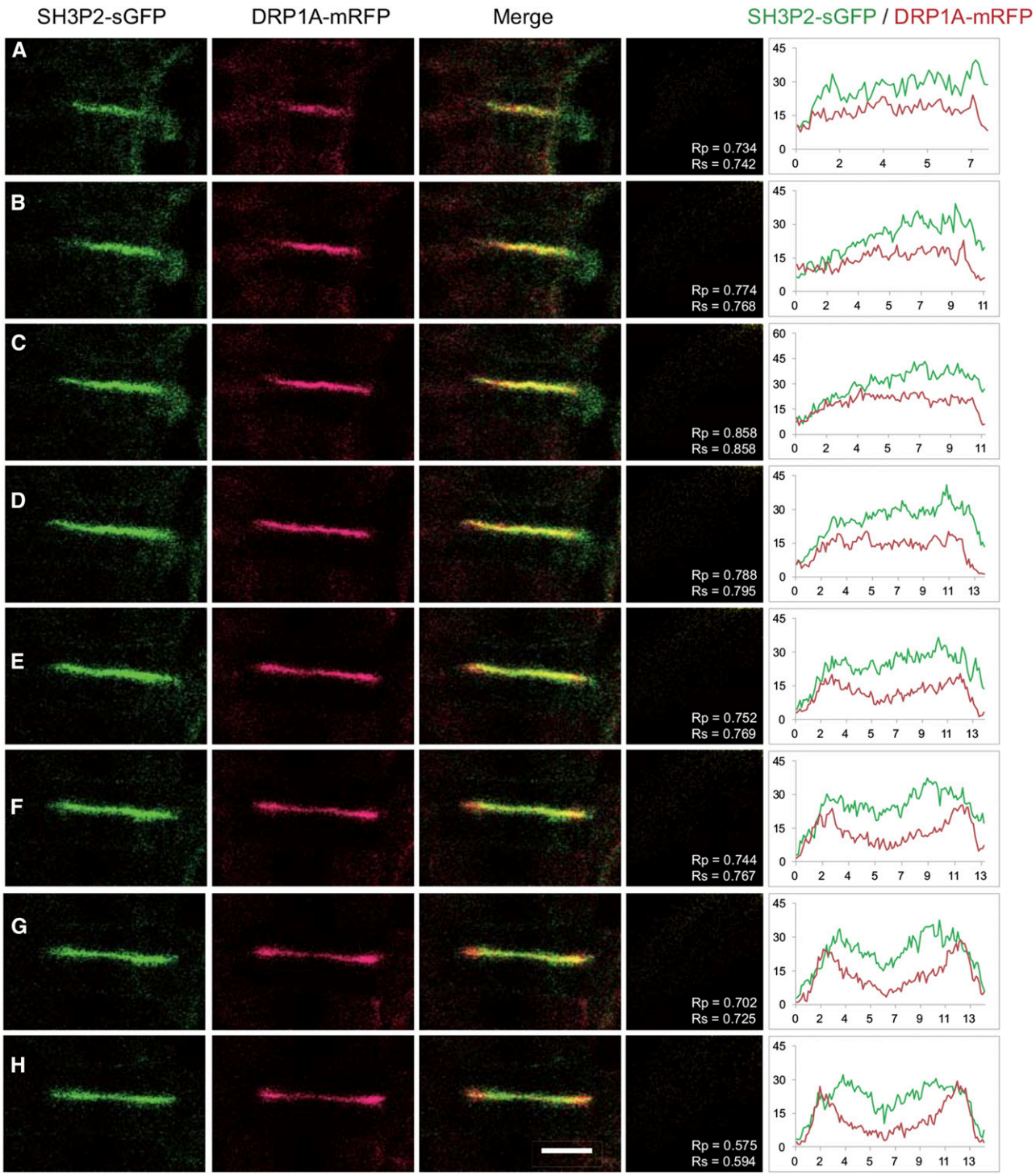

Figure 3. SH3P2 Colocalizes with DRP1A at the Leading Edges of the Cell Plate.

The localization of SH3P2-sGFP expressed under the control of the CaMV 35S promoter was compared with that of DRP1A-mRFP at the cell plate during cytokinesis. Serial optical Z-section images were obtained at 1-μm intervals from a dividing cell in root tissues of transgenic plants expressing both *SH3P2-sGFP* and *DRP1A-mRFP*. The extent of colocalization between green and magenta fluorescent signals was analyzed by ImageJ to obtain Pearson-Spearman correlation coefficients for localization. The resulting scatterplots are shown with r_p and r_s values. The level of colocalization ranges from +1 for perfect colocalization to −1 for negative correlation. In graphs, the *y* axis shows the fluorescent intensity of SH3P2-sGFP (green) and DRP1A-mRFP (magenta) at the cell plate and the *x* axis is distance (μm). Bar = 5 μm.

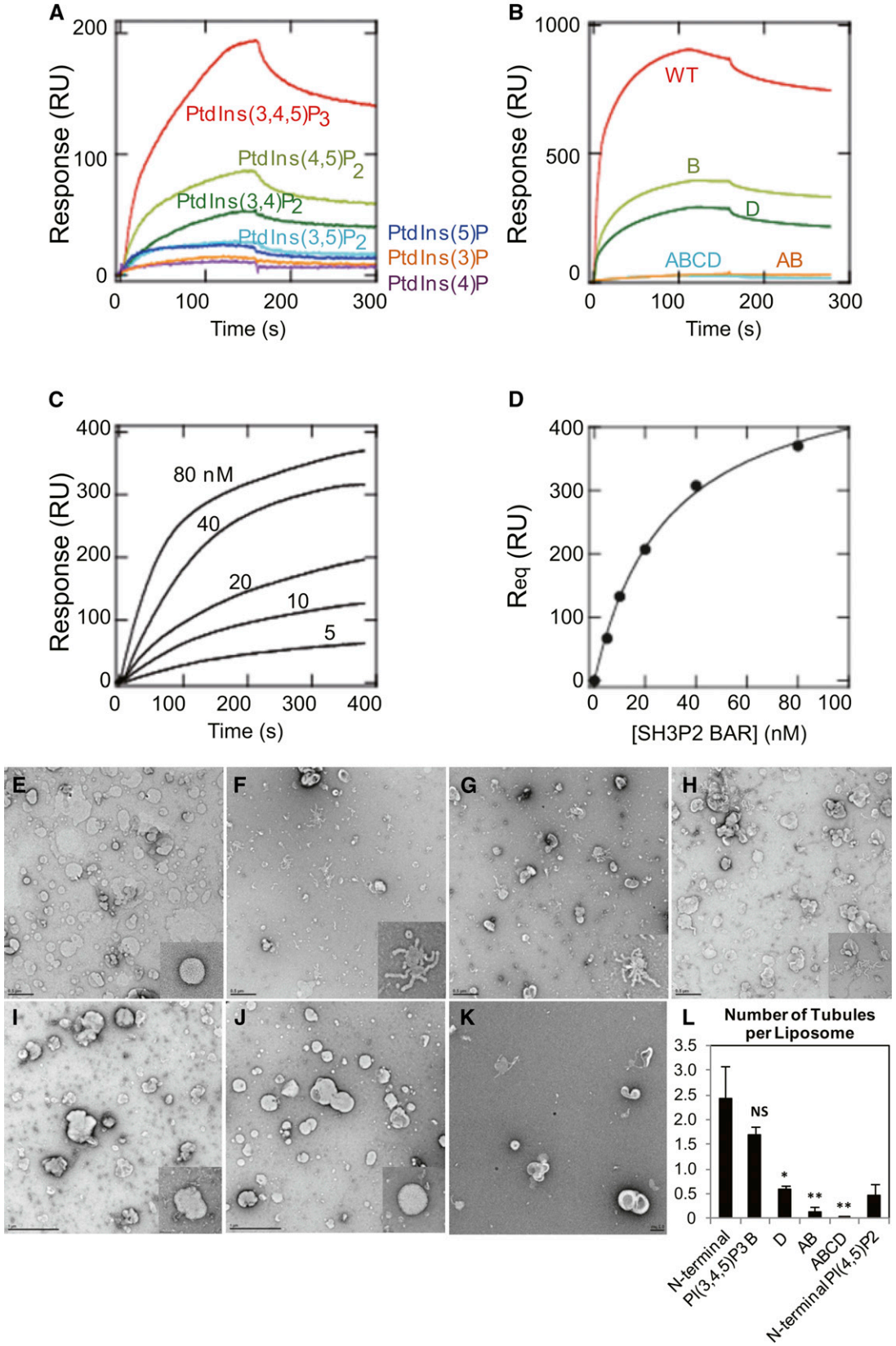

Figure 4. The SH3P2 BAR Domain Binds to PtdInsPs and Induces Tubulation of Liposomes.

(A) to **(D)** The PtdInsPs binding specificity of the SH3P2 BAR domain.

be more physiologically relevant in plants, we incubated the SH3P2 BAR domain with PI(4,5)P_2-containing liposomes. Tubulation was detectable in the presence of PI(4,5)P_2 (Figures 4K and 4L), but to a lesser extent than that of PI(3,4,5)P3, with an average of 0.48 tubules per liposome. This good correlation between the binding affinity for anionic vesicles and vesicle tubulation activity indicates that the N-terminal region of SH3P2 contains a genuine BAR domain with vesicle tubulation activity.

The in vitro study of the activity of the SH3P2 BAR domain raises the possibility that SH3P2 plays a role in tubulation of membrane structures during cell plate formation. Indeed, tubular structure formation is an essential step for generating planar plasma membranes from the incoming vesicles, and multiple types of tubular structures with different diameters are transiently produced during cell plate formation (Otegui et al., 2001; Seguí-Simarro et al., 2004). To further test this idea, we performed immunoelectron microscopy of Arabidopsis root meristem cells with the SH3P2 antibody. SH3P2-specific immunogold particles were detected at the cell plates (Supplemental Table 1). In agreement with the fluorescence microscopy results, immunogold particles were enriched in the growing region of the cell plate, often at constricted sites (Figures 5A and 5B). We examined meristem cell sections labeled with the anti-SH3P2 antibody using electron tomography to determine the localization of SH3P2 in more detail (Figures 5C to 5E'). Immunogold particles are seen in TVN membranes associated with phragmoplast microtubules where the cell plate actively expands (Figures 5C and 5D). Within the growing regions of the cell plate, SH3P2 immunogold particles are preferentially associated with narrow tubules consisting of curved membranes, at the expanding edge of the cell plate (Figures 5E and 5E'). This result suggests that SH3P2 is involved in the membrane dynamics that constructs the cell plate from TGN-derived vesicles. This notion is further supported by the phenotype of DEX-treated *SH3P2* RNAi plants that had bulky leading edges of the cell plate (Figure 1E); membrane tubulation causes a reduction in the volume by ~50% (Seguí-Simarro et al., 2004). These results suggest that SH3P2 is involved in tubulation of the vesicular membranes in the actively growing region of the cell plate. Since the cell plate stubs were rarely found in *SH3P2* RNAi plants grown under the DEX-inducible condition (Supplemental Figure 4), we could not directly monitor the effect of *SH3P2* RNAi on cell plate formation by EM.

SH3P2 Forms a Complex with DRP1A at the Cell Plate

In endosomal trafficking of animal cells, endophilin, which has a BAR and SH3 domain, regulates dynamin function either positively or negatively for budding of clathrin-coated vesicles. Tubulation induced by the BAR domain facilitates dynamin-catalyzed membrane fission in vesicle generation; on the other hand, the SH3 domain directly interacts with the PRD (proline/arginine-rich domain) of dynamin and inhibits scaffold assembly (Sundborger et al., 2011; Neumann and Schmid, 2013). Thus, the colocalization of SH3P2 with DRP1A raises the possibility that these proteins function together during cell plate formation. SH3P2 may regulate the activity of DRP1A during cell plate formation. However, DRP1A does not contain a PRD. Thus, one possible scenario is that SH3P2 indirectly interacts with DRP1A through a mediator. Plants contain six distinct DRP family members (DRP1–DRP6). Of these proteins, DRP2 has a PRD and colocalizes with DRP1 at the leading edge of the growing cell plate (Hong et al., 2003; Fujimoto et al., 2008). Moreover, DRP2 forms a heterodimer with DRP1 (Fujimoto et al., 2010). Thus, SH3P2 may interact with DRP1 via DRP2. But, among the three SH3Ps in Arabidopsis, only SH3P3 interacts with the PRD of DRP2A through the SH3 domain and inhibits the GTPase activity of DRP2A (Lam et al., 2002). Therefore, SH3P3 may mediate the interaction between SH3P2 and the DRP1/DRP2 heterodimer. To test this possibility, we first examined whether SH3P2 interacts with SH3P3 using yeast two-hybrid experiments. All three SH3Ps formed homodimers and SH3P2 also formed a heterodimer with SH3P3 (Supplemental Figure 5), indicating that SH3P2 has the potential to form a complex with SH3P3/DRP2/DRP1 through direct interaction.

To investigate the existence of the SH3P2/SH3P3/DRP2/DRP1 complex in vivo, we performed coimmunoprecipitation using protein extracts from transgenic plants expressing SH3Ps-sGFP. GFP fusion proteins were precipitated using an anti-GFP antibody, and the presence of DRP1A in the immunoprecipitates was analyzed by immunoblotting using an anti-DRP1A antibody. In previous studies,

Figure 4. (continued).

(A) His:SH3P2-BAR (100 nM) purified from *E. coli* extracts was used to determine PtdInsP selectivity by kinetic SPR analysis. The control and active surfaces of the L1 sensor chip were coated with POPC and POPC/POPS/PtdInsPs (77:20:3) vesicles, respectively. PtdInsPs include PtdIns(3,4,5)P_3, PtdIns(4,5)P_2, PtdIns(3,5)P2, PtdIns(3,4)P_2, PtdIns(5)P, PtdIns(4)P, and PtdIns(3)P.

(B) Kinetic SPR sensorgrams of binding of wild-type SH3P2 BAR domain and mutants to POPC/POPS/PtdIns(3,4,5)P_3 (77:20:3) vesicles. One-site mutants (B and D) showed ~40% of the response of wild-type protein, whereas the two-site (AB) and four-site (ABCD) mutants had negligible lipid binding.

(C) Equilibrium SPR sensorgrams for binding of SH3P2-BAR wild type to POPC/POPS/PtdIns(3,4,5)P_3 (77:20:3) vesicles. The concentration was varied from 0 to 80 nM and a near-equilibrium R value (Req) for each concentration was determined.

(D) Determination of K_d by nonlinear least-squares analysis of Req versus (SH3P2-BAR) using the equation Req = Rmax/(1 + K_d/P0). The curve fitting yielded K_d = 29 ± 2 nM and Rmax = 512 ± 19, and the theoretical curve was constructed using these parameters. All SPR measurements were performed in 20 mM Tris-HCl, pH 7.4, containing 160 mM KCl.

(E) to **(K)** Electron microscopy analysis of liposome tubulation by the N-terminal BAR domain and respective mutations of SH3P2. TEM of negative-stained liposomes after incubation for 20 min with 2 μM N-terminal SH3P2 protein and its mutants/ Liposomes alone [PC:PE:PI(3,4,5)P3, 77:20:3] **(E)** or together with N-terminal SH3P2 **(F)**, B mutant **(G)**, D mutant **(H)**, AB mutant **(I)**, or ABCD mutant **(J)**. N-terminal SH3P2 with PI(4,5)P2 liposomes [PC:PE:PI(4,5)P2] **(K)**.

(L) Quantification of tubules formed by the N-terminal domain of SH3P2 and each N-terminal domain mutant. At least three TEM images from each grid were used for quantification of formed tubules. NS, not significant; *P value < 0.03 and **P value < 0.013. A Student's *t* test was performed to determine the P value for each mutation with respect to wild-type N-terminal SH3P2.

Bars = 0.5 μm in **(E)** to **(H)**, 1 μm in **(I)** and **(J)**, and 0.2 μm in **(K)**. Error bars indicate the SE of the mean.

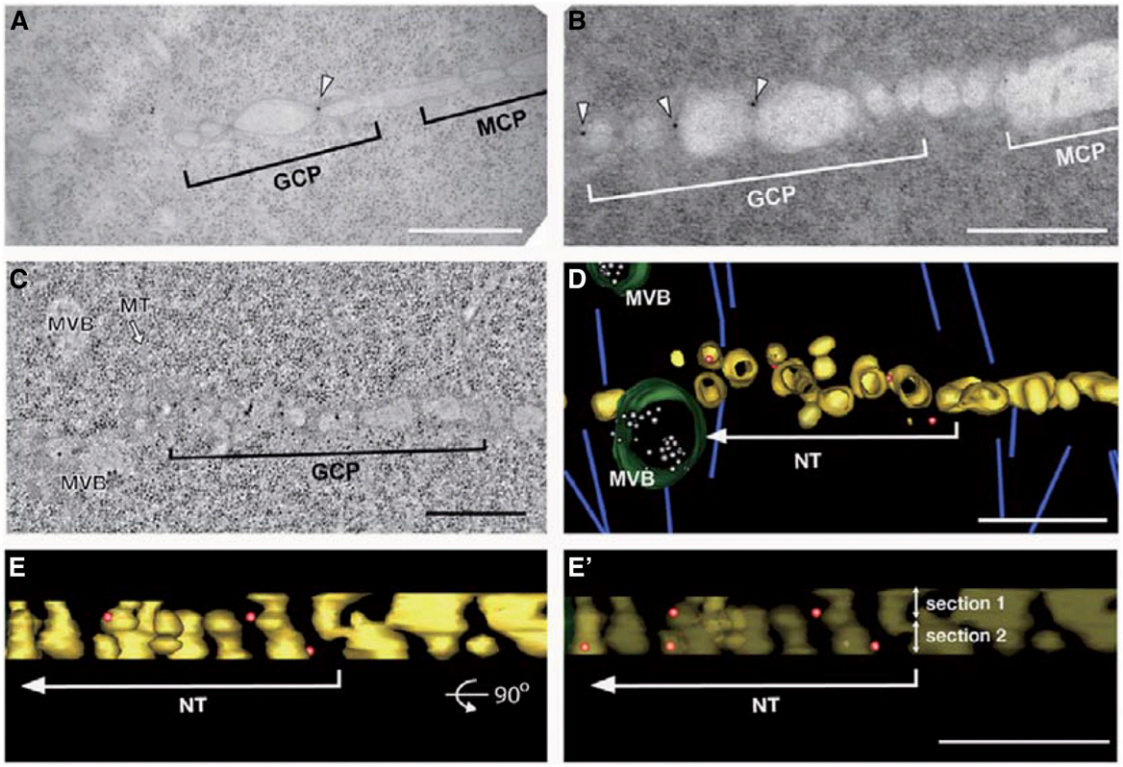

Figure 5. SH3P2 Localizes to the Constricted or Curved Regions of Membranes at the Growing Region of the Cell Plate.

(A) and **(B)** Electron micrographs of Col-0 root meristem cell sections labeled with the anti-SH3P2 antibody. Immunogold particles (arrowheads) are preferentially associated with the growing region of the cell plate (GCP) rather than the maturing region (MCP).

(C) and **(D)** A slice image from an electron tomogram showing an expanding cell plate and 3D model of the cell plate (gold), multivesicular body (MVB), and microtubule (MT) based on the tomogram. The tomogram consists of two consecutive sections (100 nm) labeled with the anti-SH3P2 antibody. Immunogold particles (red spheres) are associated with the narrow tubules (NT) of the cell plate. Arrow indicates the direction of the growing cell plate. Additional slice images are shown in Supplemental Figure 8.

(E) and **(E')** Top-down views of the cell plate model in **(D)** after rotating 90°. The cell plate membrane is rendered translucent to reveal immunogold particles in **(E')**. Reconstructed volumes from the two sections (section 1 and section 2) are marked in **(E')**. Bars = 0.5 μm.

coimmunoprecipitation and liquid chromatography-tandem mass spectrometry analyses showed that SH3P1 is a component of DRP1A and PIN1 complexes (Mravec et al., 2011). DRP1A was coprecipitated with SH3P1-sGFP and SH3P2-sGFP, but not with SH3P3-sGFP, indicating that SH3P2 forms a complex with DRP1A in an SH3P3-independent manner (Figure 6A).

We further examined whether SH3P2 forms a complex with DRP1A at the cell plate by bimolecular fluorescence complementation (BiFC) analysis. A similar approach was used to reveal the interaction between DRP1A and PIN1 at the cell plate (Mravec et al., 2011). SH3P2 and DRP1A were fused with the N- and C-terminal halves of VENUS (NV and CV), respectively. Their reciprocal constructs were also generated (Supplemental Figure 6A). These constructs as well as their control constructs, NV and CV alone, were used to generate transgenic plants. These transgenic lines expressing individual constructs were crossed to generate transgenic plants expressing both NV and CV fusion proteins. Homozygous lines were selected, and expression of these fusion proteins was examined by immunoblot analysis using an anti-GFP antibody. These fusion proteins were expressed at equal levels (Supplemental Figure 6C). VENUS fluorescent signals were observed at the cell plate from the early stages of cell plate formation in transgenic plants expressing both *SH3P2-NV* and *DRP1A-CV* or transgenic plants expressing both *DRP1A-NV* and *SH3P2-CV* (Figure 6B). However, VENUS signals were not detected in plants expressing control constructs (Supplemental Figure 6B). These results indicate that SH3P2 forms a complex with DRP1A at the cell plate.

SH3P2 Plays a Crucial Role in Localizing DRP1A to the Cell Plate after Fusion of the Incoming Vesicles

To elucidate the meaning of the interaction between SH3P2 and DRP1A in cell plate formation, we monitored the behavior of both YFP-RabA2 and DRP1A-mRFP in DEX-treated *SH3P2* RNAi plants. During cytokinesis, RabA2 traffics to the cell plate together with the incoming vesicles from the TGN and is involved in fusion of the incoming vesicles at the growing edge of the cell plate, thus playing a role in the very early step of cell plate formation (Chow et al., 2008). In DEX-treated *SH3P2* RNAi plants, YFP-RabA2 was

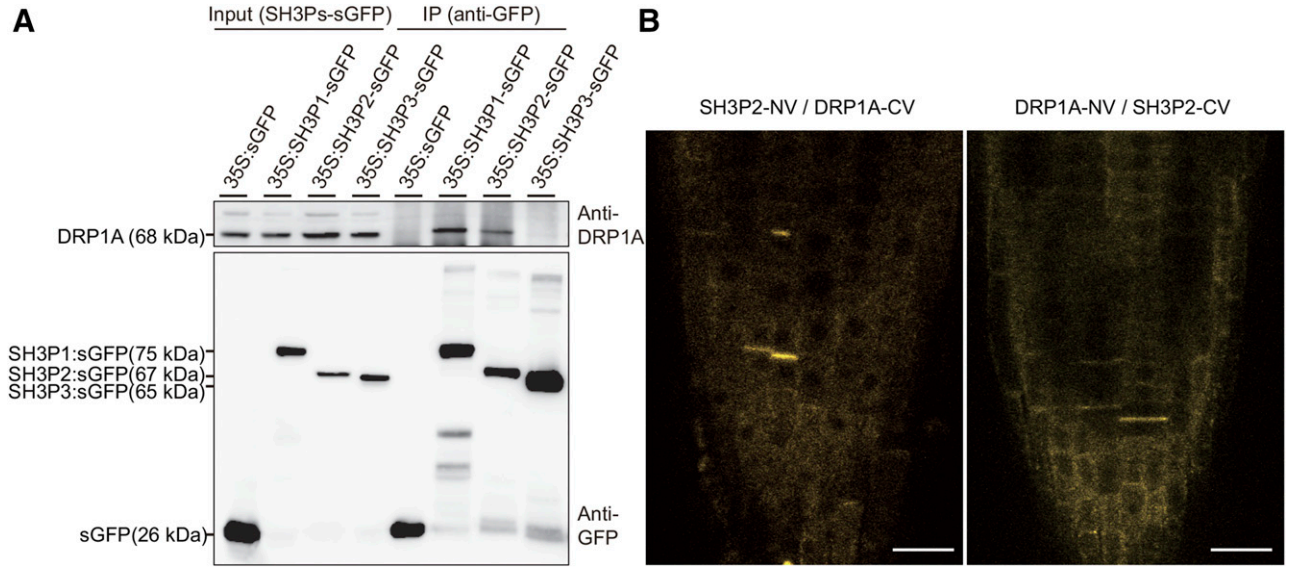

Figure 6. SH3P2 Forms a Complex with DRP1A at the Cell Plate in Dividing Cells.

(A) Interaction of SH3P1 and SH3P2 with DRP1A. Protein extracts (Input) from 5-d-old seedlings of the indicated transgenic plants were immunoprecipitated (IP) with an anti-GFP antibody. The immunoprecipitates were analyzed by immunoblotting using anti-DRP1A and anti-GFP antibodies.

(B) Interaction of SH3P2 with DRP1A at the cell plate. Root tissues of 5-d-old seedlings of transgenic plants expressing the indicated constructs were examined under a confocal laser scanning microscope. SH3P2 and DRP1A were fused with the N- and C-terminal halves of VENUS (NV and CV), respectively, and vice versa. Bars = 20 μm.

normally targeted to the cell plate and accumulated largely at the growing ends of the cell plate, similar to that in control plants, although the cell plate showed an abnormal morphology in DEX-treated *SH3P2* RNAi plants at later time points (Figure 7A). These results indicate that SH3P2 does not play a role in localizing RabA2 to the cell plate. On the other hand, the localization pattern of DRP1A-mRFP completely differed between DEX-treated and DEX-untreated *SH3P2* RNAi plants; DRP1A-mRFP was not properly targeted to the cell plates but accumulated at a distance from the cell plate in DEX-treated *SH3P2* RNAi plants, in contrast to its accumulation to the cell plate in control plants (Figure 7B), indicating that SH3P2 affects the localization of DRP1A to the cell plate.

To further understand the behavior of SH3P2 at the cell plate, we measured the time required for fluorescence recovery after photobleaching (FRAP) of SH3P2-sGFP, YFP-RabA2, and DRP1A-mRFP. In wild-type plants, the half-time of DRP1A-mRFP recovery to the cell plate after photobleaching was 10.7 s, which was faster than that (43.8 s) of YFP-RabA2. The half-time of SH3P2-sGFP recovery was 17.6 s, only slightly slower than that of DRP1A-mRFP, but much faster than that of YFP-RabA2 (Figure 8), indicating that the targeting mechanism of SH3P2 to the cell plate is similar to that of DRP1A but different from that of RabA2. Unlike RabA2, which moves to the cell plate through vesicle trafficking (Chow et al., 2008), both SH3P2 and DRP1A may be directly targeted to the cell plate from the cytosol. Taken together, these results suggest that RabA2/A3-positive vesicles derived from the TGN accumulate and fuse to each other via KNOLLE-containing complexes and both SH3P2 and DRP1A targeted to the cell plate from the cytosol play a role in membrane tubulation during cell plate formation (Figure 9).

DISCUSSION

In plants, cell plate formation is a complex process involving a series of events starting from homotypic fusion of vesicles largely derived from the TGN, tubulation of the fused vesicles to TVNs, and finally maturation to the plasma membrane through intermediate structures such as the tubular network and PFS (Otegui et al., 2001; Seguí-Simarro et al., 2004; Lukowitz et al., 1996; Chow et al., 2008). A large number of proteins have been identified that are required for various stages of cell plate formation. Their spatial and temporal localization patterns provide a clue as to their role during cell plate formation (Song et al., 2012; Park et al., 2014). SH3P2 colocalized with KNOLLE and DRP1A at the rim of the cell plate. KNOLLE, a cell plate-specific SNARE, is involved in fusion of incoming vesicles, and DRP1A plays a role in tubulation of the homotypically fused vesicles to generate TVNs (Otegui et al., 2001; Lukowitz et al., 1996). In addition, SH3P2 also colocalized with CLC at the central region of the cell plate. CLC is involved in endocytosis from the cell plate for maturation. Therefore, it is possible that SH3P2 could make various protein complexes at the cell plate depending on the stage of cell plate formation. This idea is consistent with the fact that BAR domain-containing proteins often function as a scaffold protein (Peter et al., 2004; Frost et al., 2008). The physiological role of SH3P2 shown in this study is different from its role in autophagosome formation shown by previous studies (Zhuang et al., 2013). Thus, SH3P2 appears to be involved in multiple processes depending on the stage of the cell cycle: autophagosome assembly in non-dividing cells and cell plate formation in dividing cells. Currently,

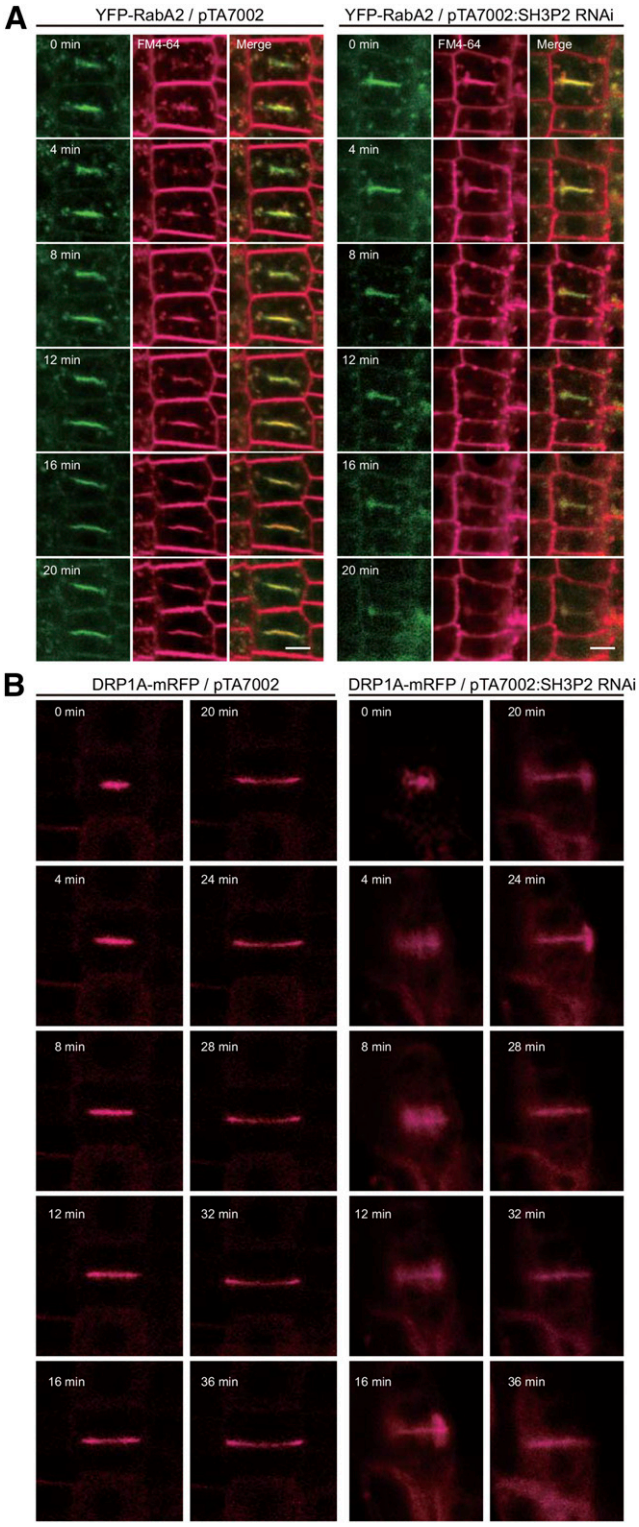

Figure 7. Cell Plate-Targeted DRP1A Accumulates around, but Is Not Targeted to, the Leading Edges of the Cell Plate in *SH3P2* RNAi Plants.

(A) and **(B)** Targeting of YFP-RabA2 and DRP1A-mRFP to the cell plate. The indicated transgenic plants were grown on 0.5× MS plates vertically in the presence of DEX (10 μM) for 5 d. The targeting of YFP-RabA2 **(A)** and DRP1-mRFP **(B)** was examined at the indicated time points under a confocal laser scanning microscope. Magenta fluorescent signals in **(A)** were generated by FM4-64 staining. Bar = 5 μm.

(B) The zero time point image of *DRP1A-mRFP/pTA7002:SH3P2* RNAi plants was collected at the scan format of 512 × 512, whereas the other images (4–36 min) were collected at the scan format of 1024 × 1024. The image at the zero time point was enlarged to a similar size as images at other time points and then processed post-collection. Serial optical Z-section images of DRP1A-mRFP/pTA7002:SH3P2 RNAi plants upon DEX treatment (4 min) are displayed in Supplemental Figure 7A.

however, it is not known how SH3P2 can play distinct roles in different cellular processes depending on the cellular conditions.

Sequence analysis shows that SH3P2 has an SH3 domain at the C-terminal region. It was originally identified as a domain that binds to the PRD of dynamins in animal cells (Gout et al., 1993), thereby regulating the activity of dynamins. Indeed, its isoform, SH3P3, interacts with DRP2A, a DRP involved in vacuolar trafficking at the TGN, and regulates its activity in vitro (Lam et al., 2002; Jin et al., 2001). Thus, SH3P2 may also play a role in cell plate formation via interaction and/or regulation of DRPs. This idea was supported by the colocalization of SH3P2 with DRP1A at the cell plate and their interaction detected by coimmunoprecipitation and BiFC analysis. However, the results of yeast two-hybrid screening suggest that SH3P2 does not directly interact with DRP1A. In fact, DRP1A does not contain a PRD that is involved in the interaction with the SH3 domain. Thus, a mediator may be involved in the interaction. DRP1A was proposed to form a heterocomplex with DRP2A (Fujimoto et al., 2010). Thus, SH3P2 may interact with DRP2A of the heterodimer of DRP1A/DRP2A mediated by SH3P3. However, in plants, DRP1A forms a complex with SH3P2, but not SH3P3. The mechanism by which SH3P2 forms a complex with DRP1A remains unknown. Currently, we can envision various possibilities for the interaction; these include involvement of other mediator proteins or membrane lipid-mediated interaction of SH3P2 and DRP1A. A previous study showed that TASH3, another SH3 domain-containing protein, is linked to the TPLATE adaptor complex involved in clathrin-mediated endocytosis and interacts with DRP1A, DRP1C, DRP1E, DRP2A, and DRP2B. In addition, TASH3 has the armadillo-type fold. Thus, TASH3 is well suited to binding to large substrates such as proteins (Gadeyne et al., 2014). It is possible that TASH3 could mediate the interaction between SH3P2 and DRP1A.

Another important domain of SH3P2 is the N-terminal BAR domain. Dimeric BAR domains bind to negatively charged lipid membranes and induce curvature in the bound membranes. They can thereby induce tubulation of lipid vesicles in vitro. Among these BAR domain proteins, endophilin functions together with dynamins to facilitate vesicle formation during endocytosis in animal cells (Sundborger et al., 2011). SH3P2 is structurally similar to endophilin with its N-terminal BAR domain and C-terminal SH3 domain. Our data also showed that the BAR domain of SH3P2 is functionally similar to that of endophilin A1 (Yoon et al., 2012) in that the isolated BAR domain of SH3P2 showed tubulation activity in vitro. These similarities raise the possibility that SH3P2 functions in concert with DRPs in cell plate formation. However,

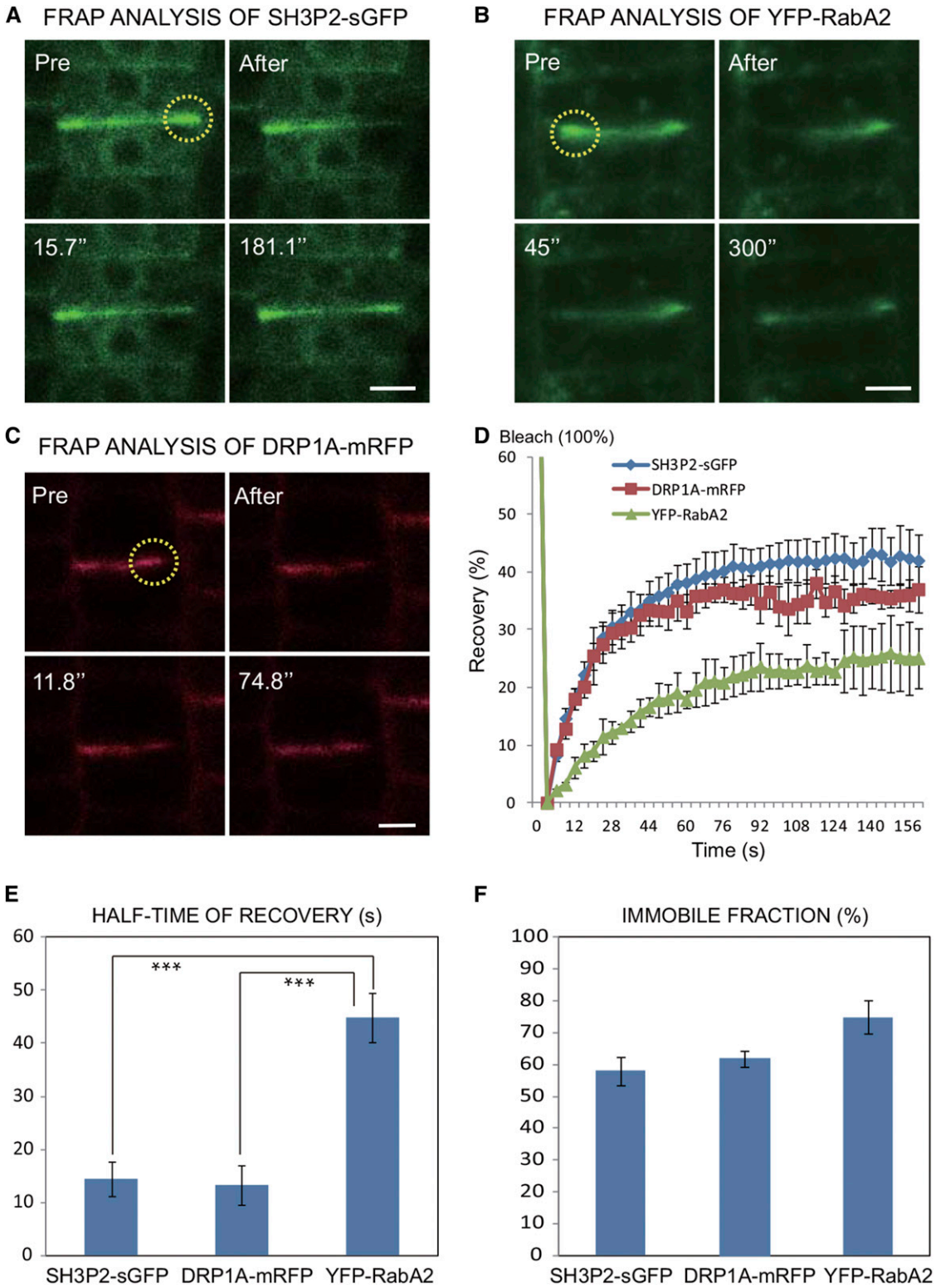

Figure 8. The Rate of Cell Plate Targeting of SH3P2 Is Similar to That of DRP1A, but Not to That of RabA2.

(A) to **(C)** FRAP analysis of SH3P2, DRP1A, and RabA2 targeting to the cell plate. SH3P2 was expressed under the control of the CaMV 35S promoter. The leading edge of the cell plate indicated by the yellow dotted circle was photobleached with a high-intensity 488-nm laser. Images were obtained before and

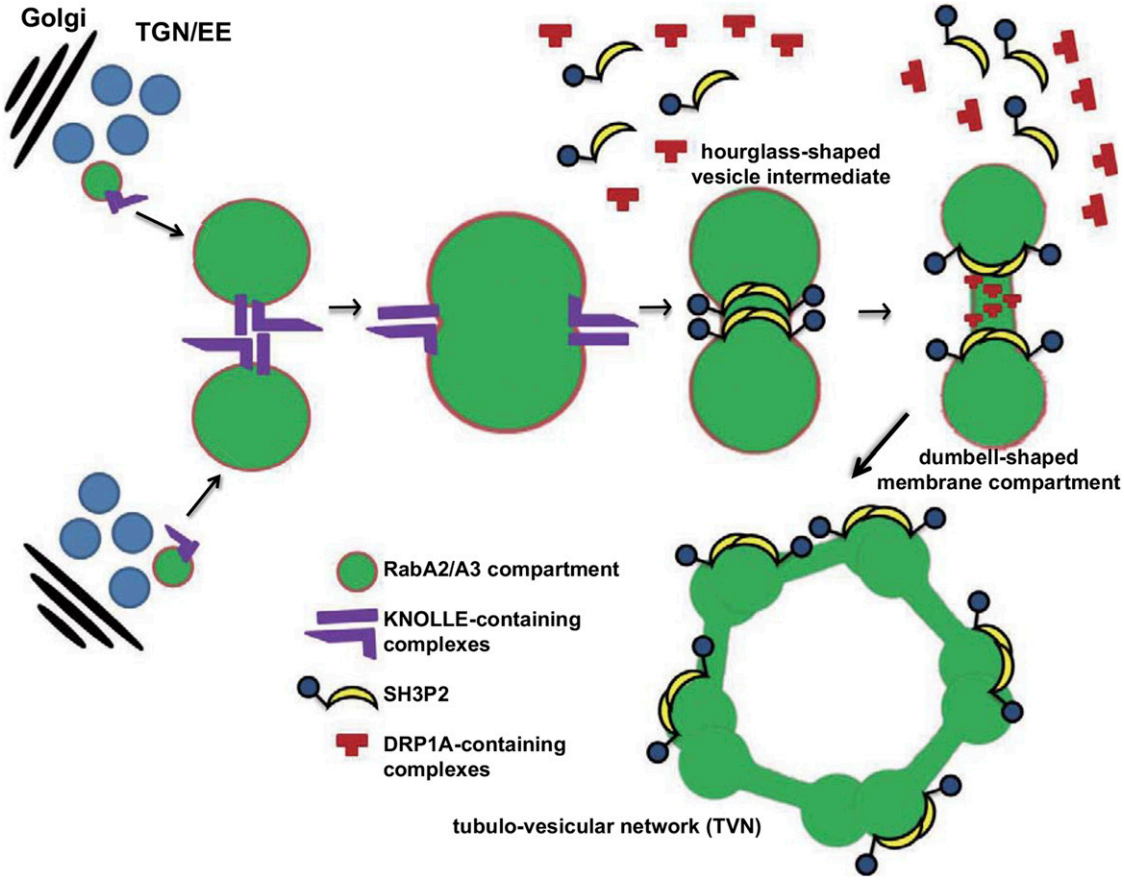

Figure 9. Schematic Model of the Proposed Role of SH3P2 and DRP1A in Cell Plate Formation during Cytokinesis in Arabidopsis.

RabA2/A3-positive vesicles derived from the TGN accumulate and fuse to each other via KNOLLE-containing complexes at the center of the dividing cell. SH3P2 contributes to the tubulation of the fused vesicular compartment to produce the hourglass-shaped intermediate. This hourglass-shaped intermediate is further constricted by DRP1A-containing complexes to form the dumbbell-shaped membrane compartment, which is the building block of the TVN. SH3P2 may also play a role in a later step during maturation of the cell plate.

endophilin and SH3P2 differ functionally in one respect: Endophilin and dynamin function in membrane scission, whereas DRP1A-SH3P2 may induce only membrane tubulation. The BAR domain of SH3P2 showed the highest binding affinity to PtIns(3,4,5)P_3. Currently, however, it is not known whether plant cells contain PtIns(3,4,5)P_3. The BAR domain of SH3P2 also has a high affinity for PtdIns(4,5)P_2, which is present in membranes of plant cells. The BAR domain was able to produce tubules from PtdIns(4,5)P_2 liposomes in vitro, albeit at a lower degree. Thus, it should be able to perform its membrane-deforming activity even if there is no PtdIns(3,4,5)P_3 under physiological conditions. It should be noted that MBP-tagged full-length (FL) SH3P2 was reported to bind to PtdIns(3)P in a qualitative lipid overlay assay (Zhuang et al., 2013) that is known to have low sensitivity and poor reliability unless the lipid blots are freshly and carefully prepared (Dowler et al., 2002). To determine the origin of the discrepancy, we expressed and purified the MBP-SH3P2 FL as described by Zhuang et al. (2013) and measured its lipid binding by SPR analysis. First, we noticed that MBP-SH3P2 FL was less stable and showed lower membrane affinity than the BAR domain, as indicated by the lower response (RU) values for binding (Supplemental Figure 3E). Second, MBP-SH3P2 FL showed much

Figure 8. (continued).

after photobleaching at a time interval of 1 s. Images show prephotobleaching (upper left), after photobleaching (upper right), half-time recovery (lower left), and saturation (lower right). Bars = 5 μm.

(D) Quantitative analysis of FRAP recovery of **(A)** to **(C)**. Error bars indicate the SD (n = 20).

(E) and **(F)** Comparison of immobile fractions **(E)** and half-time recovery **(F)** from measurements in **(D)**. Asterisks indicate a significant difference from the corresponding control experiment by the Student's t test (***P < 0.001). Error bars represent the SD (n = 20).

lower PtdInsP specificity than the BAR domain. Consistent with the report by Zhuang et al. (2013), MBP-SH3P2 FL showed a significant degree of binding to phosphatidylinositol monophosphates, including PtdIns(3)P; however, MBP-SH3P2 FL still prefers PtdIns(3,4,5)P_3 to PtdIns(3)P. Different PtdInsP binding properties of the MBP-SH3P2 FL and the BAR domain may suggest that the BAR domain is not fully exposed in the bacterially expressed MBP-SH3P2 FL, potentially due to the presence of the MBP tag. In most BAR domain-containing proteins, BAR domains are fully exposed and functional (Daumke et al., 2014). It is thus possible that bacterially expressed MBP-SH3P2 FL does not represent endogenous SH3P2 in plant cells that may bind the membrane differently from MBP-SH3P2 FL due to proper folding and posttranslational modification.

What is the exact role of SH3P2 in cell plate formation? At the initial stage of cell plate formation, incoming vesicles fuse to each other and are then converted to TVNs, which are intermediates to generate a PFS. In this mechanism, a critical process is tubulation of the fused vesicles. Previous EM studies showed that two types of vesicular structures, small-dark (~51 nm in diameter) and large-light (~66 nm in diameter) vesicular structures, are observed in the actively growing regions of the cell plate. The large-light vesicular structures derived from the fusion of two small-dark vesicular structures are modified to the hourglass-shaped intermediates, which become dumbbell-shaped membrane compartments (Otegui et al., 2001; Seguí-Simarro et al., 2004). DRP1A is proposed to play a role in tubulation. In fact, dynamins can polymerize to generate ring-like structures on the surface of lipid membranes, thereby inducing tubulation of liposomes. Previous EM gold labeling experiments showed that DRP1A localizes to the constricted neck region of the tubular structure (Otegui et al., 2001), supporting its involvement in tubulation. However, a recent study showed that DRP1A alone cannot induce tubulation of liposomes in vitro (Backues and Bednarek, 2010). By contrast, in this study, we showed that the BAR domain of SH3P2 can induce tubulation of liposomes in vitro. Thus, one possible scenario is that SH3P2 functions together with DRP1A to generate tubular structures from the fused vesicular membrane structures. Indeed, endophilin with both SH3 and BAR domains induces curvature of the neck of clathrin-coated pits to promote binding of dynamin during endocytosis (Sundborger et al., 2011). An alternative scenario is that SH3P2 and DRP1A may function sequentially to convert the fused vesicles to TVNs. Consistent with this second scenario, tubules generated by BAR domains and dynamins differ in their diameter; BAR domains produce tubules with a diameter of 15 to 80 nm, whereas dynamins produce tubules with a diameter of ~10 nm (Mim et al., 2012; Mears et al., 2007; Yin et al., 2009; Faelber et al., 2012). Considering the size of tubules and the properties of dynamins and BAR domains, SH3P2 could be involved in generating the hourglass-shaped intermediates (~45 nm in diameter) from the large-light vesicles. This hourglass-shaped intermediate is further constricted to tubules with a diameter of ≤20 nm by dynamin-like rings to generate dumbbell-shaped structures, which are the building blocks of the TVN (Otegui et al., 2001; Seguí-Simarro et al., 2004). The phenotype of *SH3P2* RNAi plants (i.e., cell plates that were less well defined but leading edges that were bulky) and the fact that DRP1A was not properly targeted to the cell plate in RNAi plants are consistent with both scenarios. Although high-resolution EM images of cell plate stubs in *SH3P2* RNAi plants can help distinguish these two possibilities, we were not able to obtain images of cell plate stubs in the EM sections of roots because the cell plate stubs were rarely found in these *SH3P2* RNAi plants grown under the DEX-inducible conditions. However, we did observe defects at the edges of the cell plate in *SH3P2* RNAi plants, indicating that suppression of the SH3P2 level hampers the generation of cell plates at the initial stage but does not fully abrogate membrane tubulation that involves other proteins, such as DRP1A.

In summary, SH3P2 localizes to the cell plate, in particular at the growing rim of the cell plate. In fact, it localized to the constricted part of the actively growing region of the cell plate. Moreover, SH3P2 affects location of DRP1A to the cell plate and forms a complex with DRP1A, which is involved in tubulation of the fused vesicles. Based on these results, we propose that SH3P2 functions together with DRP1A in the tubulation of the fused vesicles to generate the TVN at the growing region of the cell plate in dividing cells.

METHODS

Plant Growth Conditions

Arabidopsis thaliana plants (ecotype Col-0 and Ws-2) were grown on 0.5× Murashige and Skoog (MS) plates with 1% sucrose and 0.8% agar and at pH 5.7 in a growth chamber (white fluorescent lamps and a photon flux intensity of 100 μmol m^{-2} s^{-1}) at 20 to 22°C under a 16-h-light/8-h-dark cycle. To observe fluorescent proteins from root tissues, seedlings were vertically grown on 0.5× MS plates in the presence and absence of 10 μM DEX for 5 d. To check protein levels, seedlings were harvested and frozen immediately in liquid nitrogen.

Isolation of T-DNA Insertion Mutants and RT-PCR Analysis of Transcripts

To prepare genomic DNA from T-DNA insertion mutants of *SH3Ps*, *sh3p1* (SAIL-586-H07, Col-0), *sh3p2* (FLAG018E03, Ws-2), and *sh3p3* (Salk_065790c, Col-0), leaf tissues were homogenized in genomic DNA isolation buffer (200 mM Tris-Cl, pH 7.5, 250 mM NaCl, 25 mM EDTA, and 0.5% SDS) and used to identify a region flanking the T-DNA insertion site by a thermal asymmetric interlaced-PCR approach using the primer LB and gene-specific forward primers (P1LP for *SH3P1*, P2LP for *SH3P2*, and P3LP for *SH3P3*) or reverse primers (P1RP for *SH3P1*, P2RP for *SH3P2*, and P3RP for *SH3P3*).

Total RNA was isolated from leaf tissues of *sh3p1*, *sh3p2*, and *sh3p3* mutant plants, and *SH3Ps* transcript levels were determined by RT-PCR using the specific primers of SH3P1-P1, SH3P1-P2, SH3P1-P3, SH3P1-P4, and SH3P1-P5 for *SH3P1*; SH3P2-P1, SH3P2-P2, SH3P2-P3, SH3P2-P4, and SH3P2-P5 for *SH3P2*; and SH3P3-P1, SH3P3-P2, SH3P3-P3, and SH3P3-P4 for *SH3P3*. As a control, *18S* rRNA levels were determined using the primers 18S-5 and 18S-3 (Supplemental Table 2).

Construction of Plasmids and Generation of Transgenic Plants

To generate a native promoter-driven *SH3P2-YFP* construct, a 3.1-kb fragment of the *SH3P2* gene containing the 429-bp 5′ upstream promoter region and 2697-bp genomic sequences of the coding region except for the stop codon was isolated by PCR from Arabidopsis genomic DNA using Phusion High-Fidelity DNA polymerase and specific primers P2-1 and P2-2 (Supplemental Table 2). The entry vector pDONR201 and subsequently the

pGWB40 destination vector were used for in-frame C-terminal YFP fusion. The construct sequences were validated by nucleotide sequencing.

To generate *SH3Ps-sGFP* overexpression constructs, first the *sGFP* fragment was inserted into pCsV1300 (Invitrogen) using the *Kpn*I and *Bam*HI sites. The *SH3P* cDNAs, *SH3P1* (At1g31440), *SH3P2* (At4g34660), and *SH3P3* (At4g18060), were isolated from a cDNA library by PCR using the following gene-specific primers: P1-1 and P1-2 for *SH3P1*, P2-3 and P2-4 for *SH3P2*, and P3-1 and P3-2 for *SH3P3*. These *SH3P* cDNAs were inserted into pCsV1300:sGFP using the *Xba*I and *Kpn*I sites for *SH3P1* and *SH3P2*, and the *Spe*I and *Kpn*I sites for *SH3P3*.

For BiFC constructs, the *Spe*I-*Myc tag*-*Xba*I fragment was amplified by PCR using a set of primers, Myc-1 and Myc-2, and inserted into pCsV1300 using the *Xba*I site. The N-terminal (173 amino acids) and C-terminal (84 amino acids) regions of VENUS were amplified by PCR using the nV-1, nV-2, cV-1, and cV-2 primers. The PCR products were inserted into pCsV1300:Myc using the *Kpn*I and *Bam*HI sites. *SH3P2* and *DRP1A* cDNAs, which were amplified by PCR using the BiP2-1, BiP2-2, Bi1A-1, and Bi1A-2 primers, were inserted into pCsV1300:Myc using the *Xba*I and *Stu*I sites. Transgenic plants were generated by the floral dipping method (Clough and Bent, 1998) and screened on 0.5× MS medium containing antibiotics (30 mg/L hygromycin B and 100 mg/L cefotaxime), and homozygous plants were screened at the T3 generation. *DRP1A-mRFP* (Mravec et al., 2011) and *YFP-RabA2* (Chow et al., 2008) transgenic plants were crossed with pCsV1300:SH3P2-sGFP, pTA7002 (Aoyama and Chua, 1997), and pTA7002:*RNAi-SH3P2* (Zhuang et al., 2013) for localization experiments.

In Vivo Imaging and Immunohistochemistry

The primary roots of 5-d-old seedlings were used to perform in vivo imaging and immunohistochemistry (Park et al., 2005). Seedlings were treated with 12 μM FM4-64 for 1 min to observe the cell plate. The immunofluorescence samples were prepared as described previously (Lauber et al., 1997). The primary antibodies were anti-KNOLLE (1:500), anti-DRP1A (1:1000), and anti-CLC (1:1000). Anti-rabbit Cy3-coupled IgG (1:300; Jackson ImmunoResearch; catalog no. 711-165-152) was used as the secondary antibody. After washing, slides were mounted in Mowiol 4-88 (Calbiochem). Images were captured using a Zeiss LSM 510 META laser scanning confocal microscope and processed using the LSM 5 image browser and Adobe Photoshop 7. The combinations of excitation wavelength/emission filter were 488 nm (argon ion laser)/505 to 530 nm band-pass for GFP, 514 nm/530 to 600 nm band-pass for YFP and VENUS, and 543 nm/560 to 615 nm band-pass for mRFP and FM4-64. For statistical analysis, the PSC colocalization plug-in (French et al., 2008) for ImageJ (Abramoff et al., 2004) was used to calculate the linear Pearson correlation coefficient (r_p) and the nonlinear Spearman's rank correlation coefficient (r_s) of red and green fluorescent signals. The threshold level was set to 10. The pixel values below 10 were considered noise and excluded from the statistical analysis.

We performed FRAP experiments using a Zeiss LSM 510 META laser scanning confocal microscope. Edge regions of the cell plate were bleached with a high-intensity 488-nm laser beam, and images were captured immediately after photobleaching at time intervals of 2 s over a period of 5 min in the Time Series mode by StartB. The fluorescent recovery curves were corrected by changing of background intensity to consider the inherent imaging-related photobleaching and normalized to a value of 1 for the prebleaching ratio. The mobile fraction was determined by comparing the fluorescence in the bleached area after full recovery (F_∞) with the fluorescence before bleaching (F_i) and just after bleaching (F_0). The mobile faction R is defined as $R = (F\infty - F0) / (Fi - F0)$. (1 − R) represents the immobile fraction ratio. The half-time ($t_{1/2}$) of recovery is the time from the bleach (F_0) to the time point where the fluorescence intensity reaches half of the intensity after full recovery (F_∞).

Immunoblot Analysis and Immunoprecipitation

Protein was extracted in 20 mM Tris-Cl, pH 7.5, 40 mM NaCl, 3 mM $MgCl_2$, 0.5% Triton X-100, 1× Complete Protease Inhibitor Cocktail (Roche), and 1 mM DTT. For immunoprecipitation, rabbit anti-GFP polyclonal antibodies (2 μg; Bio-Application) were incubated with protein A agarose resin (RepilGen) and protein extracts at 4°C. Complexes were separated by SDS-PAGE and subjected to immunoblot analysis (Jin et al., 2001). Immunoblot analysis was performed using anti-GFP monoclonal (1:5000; Invitrogen; catalog no. MA5-15256), anti-Myc monoclonal (1:5000; Cell Signaling; catalog no. 2276S), and DRP1A polyclonal (Otegui et al., 2001) (1:1000) antibodies. The blots were developed using an ECL Kit (Amersham Pharmacia Biotech), and images were obtained using the LAS3000 image-capture system (FujiFilm).

Immunoelectron Microscopy and Electron Tomography

Arabidopsis (Col-0) root tip samples for immunogold labeling were prepared by high-pressure freezing and freeze substitution, and dehydrated samples were embedded in HM20 resin (Electron Microscopy Sciences) at –45°C. After polymerization, the samples were sectioned and immunolabeled with the SH3P2 antibody (Zhuang et al., 2013). These procedures were performed according to a published protocol (Kang, 2010). Tomography analysis and 3D model reconstruction were performed as described previously (Donohoe et al., 2013).

Yeast Two-Hybrid Analysis

SH3P1 cDNA was inserted into pGADT7 and pGBKT7 (BD Biosciences Clontech) using the restriction endonuclease sites *Bam*HI/*Xho*I and *Bam*HI/*Pst*I, respectively. *SH3P2* cDNA was inserted into pGADT7 and pGBKT7 using the restriction endonuclease sites *Eco*RI and *Bam*HI. *SH3P3* cDNA was inserted into pGADT7 and pGBKT7 using the restriction endonuclease sites *Eco*RI/*Xba*I and *Eco*RI/*Sal*I, respectively. The yeast strain AH109 was transformed with these constructs via PEG-mediated transformation. Transformants were plated on synthetic dropout medium (SD) without leucine to select for the presence of the pGADT7 vector and without tryptophan to select for the presence of pGBKT7 and incubated for 2 d at 30°C. Selected yeast colonies were grown in liquid YPD media and then on solid YPD plates for 2 d at 30°C. For the interaction assay, the optical density (OD_{600} = 0.4) of liquid cultures was equalized and cells were spotted on solid SD media without leucine, tryptophan, and histidine and incubated at 30°C for 2 d.

Recombinant BAR Domain Preparation

The DNA fragment encoding the BAR domain of SH3P2 (residues 1–300) was amplified by PCR and subcloned into pET-21(a). All mutations were generated by two-step extension PCR mutagenesis and verified by DNA sequencing (primers are shown in Supplemental Table 2). For protein expression, the constructs were transformed into *Escherichia coli* BL21 RIL codon plus cells (Stratagene). Cells were grown in Luria broth containing 100 μg/mL ampicillin at 37°C. When OD_{600} reached ~0.8, 0.5 mM isopropyl-β-D-1-thiogalactopyranoside was added for protein induction. Cells were grown for an additional 6 to 10 h at 25°C and harvested by centrifugation for 10 min at 4°C at 2500*g*. Cell pellets were resuspended in 50 mM Tris-HCl buffer (pH 7.4) containing 160 mM KCl, 1 mM phenylmethylsulfonyl fluoride, and 5 mM DTT. Cells were lysed by sonication, and then the lysates were centrifuged at 40,000*g* for 30 min at 4°C. Ni-NTA resin (Qiagen) was added to the supernatant, which was filtered through a 0.8-μm pore-size syringe filter (Nalgene). The mixture was poured onto a column after gentle mixing for 30 min, and then the column was washed with the abovementioned buffer containing 50 mM imidazole. BAR

domains were eluted by increasing the concentration of imidazole to 300 mM. Eluted proteins were further purified by ion-exchange and gel-filtration chromatography. The purity and concentration of proteins were assessed by SDS-PAGE and the bicinchoninic acid assay (Pierce), respectively.

Lipid Binding Affinity of the BAR Domain

POPC, POPE, and POPS were purchased from Avanti Polar Lipids, and 1,2-dipalmitoyl derivatives of PtdIns(4,5)P_2, PtdIns(3,4)P_2, PtdIns(3,5)P_2, PtdIns(3,4,5)P_3, PtdIns(5)P, PtdIns(4)P, and PtdIns(3)P were from Cayman Chemical.

All SPR measurements were performed at 23°C using a lipid-coated L1 chip in the BIACORE X system as described previously (Stahelin and Cho, 2001). Briefly, after washing the sensor chip surface with running buffer (50 mM Tris-HCl, pH 7.4, containing 160 mM KCl), POPC/POPS/PtdInsP (77:20:3%) and POPC (100%) vesicles were injected at a rate of 2 μL/min onto the active surface and control surface, respectively, to give the same resonance unit values. The level of lipid coating for both surfaces was kept at the minimum needed for preventing nonspecific adsorption to the sensor chips. This low surface coverage minimized the mass transport effect and kept the total protein concentration higher than the total concentration of protein binding sites on vesicles. Equilibrium SPR measurements were performed at a flow rate of 5 μL/min to allow sufficient time for the R values of the association phase to reach near-equilibrium values (R_{eq}). After sensorgrams were obtained for five or more different concentrations of each protein within a 10-fold range of K_d, each of the sensorgrams was corrected for refractive index change by subtracting the control surface response from it. Assuming a Langmuir-type binding between the protein (P) and protein binding sites (M) on vesicles (i.e., P + M ↔ PM), R_{eq} values were then plotted versus P_0, and the K_d value was determined by a nonlinear least-squares analysis of the binding isotherm using an equation, $Req = Rmax/(1 + Kd/P0)$. Each analysis was repeated three or more times to calculate average and SD values. For kinetic SPR measurements, the flow rate was maintained at 30 μL/min for both association and dissociation phases.

Liposome Morphology Imaging Using Transmission Electron Microscopy

Liposomes composed of PC:PE:PI(3,4,5)P_3 or PI(4,5)P_2 (77:20:3) were prepared by extrusion through 400-nm membranes. The final liposome concentration was 0.5 mM. Liposomes were allowed to incubate with 2 μM SH3P2 BAR domain or respective mutants for 20 min in a final assay volume of 100 μL. For the negative staining procedure, 3 μL of assay mixture was adsorbed onto glow-discharged formvar and carbon-coated copper EM grids for 1 min and then washed with distilled water and stained with 2% (w/v) uranyl acetate for another minute. Excess liquid was blotted dry and grids were imaged using a FEI Tecnai G2 20 transmission electron microscope at 200 kV. For the quantification of tubulation induced due to interaction of SH3P2 BAR domain with liposomes, at least three images containing more than 30 liposomes from random locations on each grid were chosen. For scoring, each independent tubule and each branch of a tubule was counted as a tubule. Degree of tubulation was expressed as number of tubules per vesicle observed. The D mutant induced formation of two different types of tubulation. One type of tubule was short and thick, similar to tubules induced by the N-terminal SH3P2 protein, while the other type of tubule was narrow and thin. Only the thick tubules that were similar to tubules induced by N-terminal SH3P2 protein were used for quantification. The narrow tubules were present in all transmission electron microscopy (TEM) images of the D mutant.

Accession Numbers

Sequence data from this article can be found in the GenBank/EMBL database or the Arabidopsis Genome Initiative database under the following accession numbers: *SH3P1*, At1g31440; *SH3P2*, At4g34660; *SH3P3*, At4g18060; *DRP1A*, At5g42080; and *RabA2*, At1g09630. Arabidopsis T-DNA insertion lines are as follows: *sh3p1* (SAIL-586-H07, Col-0), *sh3p2* (FLAG018E03, Ws-2), *sh3p3* (SALK_065790c, Col-0), and drp1a2 (SALK_069077, Col-0).

Supplemental Data

Supplemental Figure 1. Isolation of T-DNA insertion mutants of *SH3P*s.

Supplemental Figure 2. SH3P2 colocalizes with proteins that play a role at the leading edges of the cell plate during early stages of cell plate formation.

Supplemental Figure 3. Homology modeling of SH3P2 BAR and purifications of wild-type SH3P2 BAR and mutants.

Supplemental Figure 4. Cytokinesis defective phenotypes of *SH3P2* RNAi plants.

Supplemental Figure 5. SH3Ps form homomeric or heteromeric dimers depending on isoforms.

Supplemental Figure 6. Expression of BiFC constructs in transgenic plants.

Supplemental Figure 7. Characterization of the localization of DRP1A-mRFP in *SH3P2* RNAi plants.

Supplemental Figure 8. Tomographic slice images of the two sections in Figure 5 and 3D models.

Supplemental Table 1. Numbers of gold particles associated with plant organelles.

Supplemental Table 2. The nucleotide sequences of primers used in this study.

ACKNOWLEDGMENTS

This work was supported in part by the Cooperative Research program for Agriculture Science and Technology Development (Project 010953012016) "Rural Development Administration," Republic of Korea, by National Institutes of Health (NIH) Grant GM68849 to W.C., and by the Institute for Basic Science (IBS-R021-D1) to H.K. K.J.W. was funded by a CBBI fellowship supported by the NIH (T32GM075762). B.-H.K. and L.J. were supported by the Research Grants Council of Hong Kong (AoE/M-05/12 and C4011-14R). We thank Christopher Gilipin, Facility Director of the Purdue University Electron Microscopy Facility, for technical support and imaging of samples.

AUTHOR CONTRIBUTIONS

G.A. and I.H. conceived the study. G.A., R.V.S., L.J., W.C., B.-H.K., and I.H. designed the experiments. G.A., H.K., D.H.K., and H.H. performed imaging, biochemistry, and physiology experiments. Y.Y. and I.S. performed the lipid-binding assay using SPR. K.J.W. and K.A.J. performed liposome morphology imaging using TEM. X.Z. made the SH3P2 antibody. Z.L. performed the immunoelectron microscopy and electron tomography. G.A., R.V.S., L.J., W.C., B.H.K., and I.H. analyzed the data. G.A., R.V.S., W.C., B.H.K., and I.H. wrote the manuscript. All authors read, revised, and approved of the article.

Received February 7, 2017; revised April 21, 2017; accepted June 5, 2017; published June 5, 2017.

REFERENCES

Abramoff, M.D., Magelhaes, P.J., and Ram, S.J. (2004). Image processing with ImageJ. Biophotonics International **11:** 36–42.

Aoyama, T., and Chua, N.H. (1997). A glucocorticoid-mediated transcriptional induction system in transgenic plants. Plant J. **11:** 605–612.

Backues, S.K., and Bednarek, S.Y. (2010). *Arabidopsis* dynamin-related protein 1A polymers bind, but do not tubulate, liposomes. Biochem. Biophys. Res. Commun. **393:** 734–739.

Bolte, S., Talbot, C., Boutte, Y., Catrice, O., Read, N.D., and Satiat-Jeunemaitre, B. (2004). FM-dyes as experimental probes for dissecting vesicle trafficking in living plant cells. J. Microsc. **214:** 159–173.

Chow, C.M., Neto, H., Foucart, C., and Moore, I. (2008). Rab-A2 and Rab-A3 GTPases define a trans-golgi endosomal membrane domain in Arabidopsis that contributes substantially to the cell plate. Plant Cell **20:** 101–123.

Clough, S.J., and Bent, A.F. (1998). Floral dip: a simplified method for *Agrobacterium*-mediated transformation of *Arabidopsis thaliana*. Plant J. **16:** 735–743.

Collings, D.A., Gebbie, L.K., Howles, P.A., Hurley, U.A., Birch, R.J., Cork, A.H., Hocart, C.H., Arioli, T., and Williamson, R.E. (2008). Arabidopsis dynamin-like protein DRP1A: a null mutant with widespread defects in endocytosis, cellulose synthesis, cytokinesis, and cell expansion. J. Exp. Bot. **59:** 361–376.

Daumke, O., Roux, A., and Haucke, V. (2014). BAR domain scaffolds in dynamin-mediated membrane fission. Cell **156:** 882–892.

Donohoe, B.S., Kang, B.H., Gerl, M.J., Gergely, Z.R., McMichael, C.M., Bednarek, S.Y., and Staehelin, L.A. (2013). Cis-Golgi cisternal assembly and biosynthetic activation occur sequentially in plants and algae. Traffic **14:** 551–567.

Dowler, S., Kular, G., and Alessi, D.R. (2002). Protein lipid overlay assay. Sci. STKE **2002:** pl6.

El Kasmi, F., Krause, C., Hiller, U., Stierhof, Y.D., Mayer, U., Conner, L., Kong, L., Reichardt, I., Sanderfoot, A.A., and Jürgens, G. (2013). SNARE complexes of different composition jointly mediate membrane fusion in *Arabidopsis* cytokinesis. Mol. Biol. Cell **24:** 1593–1601.

Faelber, K., Held, M., Gao, S., Posor, Y., Haucke, V., Noé, F., and Daumke, O. (2012). Structural insights into dynamin-mediated membrane fission. Structure **20:** 1621–1628.

Ferguson, S.M., Raimondi, A., Paradise, S., Shen, H., Mesaki, K., Ferguson, A., Destaing, O., Ko, G., Takasaki, J., Cremona, O., O' Toole, E., and De Camilli, P. (2009). Coordinated actions of actin and BAR proteins upstream of dynamin at endocytic clathrin-coated pits. Dev. Cell **17:** 811–822. Erratum. Dev. Cell **18:** 332.

French, A.P., Mills, S., Swarup, R., Bennett, M.J., and Pridmore, T.P. (2008). Colocalization of fluorescent markers in confocal microscope images of plant cells. Nat. Protoc. **3:** 619–628.

Frost, A., Perera, R., Roux, A., Spasov, K., Destaing, O., Egelman, E.H., De Camilli, P., and Unger, V.M. (2008). Structural basis of membrane invagination by F-BAR domains. Cell **132:** 807–817.

Fujimoto, M., Arimura, S., Nakazono, M., and Tsutsumi, N. (2008). Arabidopsis dynamin-related protein DRP2B is co-localized with DRP1A on the leading edge of the forming cell plate. Plant Cell Rep. **27:** 1581–1586.

Fujimoto, M., Arimura, S., Ueda, T., Takanashi, H., Hayashi, Y., Nakano, A., and Tsutsumi, N. (2010). *Arabidopsis* dynamin-related proteins DRP2B and DRP1A participate together in clathrin-coated vesicle formation during endocytosis. Proc. Natl. Acad. Sci. USA **107:** 6094–6099.

Gadeyne, A., et al. (2014). The TPLATE adaptor complex drives clathrin-mediated endocytosis in plants. Cell **156:** 691–704.

Gao, C., Luo, M., Zhao, Q., Yang, R., Cui, Y., Zeng, Y., Xia, J., and Jiang, L. (2014). A unique plant ESCRT component, FREE1, regulates multivesicular body protein sorting and plant growth. Curr. Biol. **24:** 2556–2563.

Gao, C., Zhuang, X., Cui, Y., Fu, X., He, Y., Zhao, Q., Zeng, Y., Shen, J., Luo, M., and Jiang, L. (2015). Dual roles of an *Arabidopsis* ESCRT component FREE1 in regulating vacuolar protein transport and autophagic degradation. Proc. Natl. Acad. Sci. USA **112:** 1886–1891.

Gout, I., et al. (1993). The GTPase dynamin binds to and is activated by a subset of SH3 domains. Cell **75:** 25–36.

Hong, Z., Bednarek, S.Y., Blumwald, E., Hwang, I., Jurgens, G., Menzel, D., Osteryoung, K.W., Raikhel, N.V., Shinozaki, K., Tsutsumi, N., and Verma, D.P.S. (2003). A unified nomenclature for *Arabidopsis* dynamin-related large GTPases based on homology and possible functions. Plant Mol. Biol. **53:** 261–265.

Jin, J.B., Kim, Y.A., Kim, S.J., Lee, S.H., Kim, D.H., Cheong, G.W., and Hwang, I. (2001). A new dynamin-like protein, ADL6, is involved in trafficking from the trans-Golgi network to the central vacuole in *Arabidopsis.* Plant Cell **13:** 1511–1526.

Jürgens, G. (2005). Cytokinesis in higher plants. Annu. Rev. Plant Biol. **56:** 281–299.

Kang, B.H. (2010). Electron microscopy and high-pressure freezing of Arabidopsis. Methods Cell Biol. **96:** 259–283.

Kang, B.H., Busse, J.S., and Bednarek, S.Y. (2003). Members of the *Arabidopsis* dynamin-like gene family, ADL1, are essential for plant cytokinesis and polarized cell growth. Plant Cell **15:** 899–913.

Kolb, C., Nagel, M.K., Kalinowska, K., Hagmann, J., Ichikawa, M., Anzenberger, F., Alkofer, A., Sato, M.H., Braun, P., and Isono, E. (2015). FYVE1 is essential for vacuole biogenesis and intracellular trafficking in Arabidopsis. Plant Physiol. **167:** 1361–1373.

Lam, B.C., Sage, T.L., Bianchi, F., and Blumwald, E. (2001). Role of SH3 domain-containing proteins in clathrin-mediated vesicle trafficking in *Arabidopsis.* Plant Cell **13:** 2499–2512.

Lam, B.C., Sage, T.L., Bianchi, F., and Blumwald, E. (2002). Regulation of ADL6 activity by its associated molecular network. Plant J. **31:** 565–576.

Lauber, M.H., Waizenegger, I., Steinmann, T., Schwarz, H., Mayer, U., Hwang, I., Lukowitz, W., and Jürgens, G. (1997). The Arabidopsis KNOLLE protein is a cytokinesis-specific syntaxin. J. Cell Biol. **139:** 1485–1493.

Lukowitz, W., Mayer, U., and Jürgens, G. (1996). Cytokinesis in the *Arabidopsis* embryo involves the syntaxin-related KNOLLE gene product. Cell **84:** 61–71.

Mears, J.A., Ray, P., and Hinshaw, J.E. (2007). A corkscrew model for dynamin constriction. Structure **15:** 1190–1202.

Miart, F., Desprez, T., Biot, E., Morin, H., Belcram, K., Höfte, H., Gonneau, M., and Vernhettes, S. (2014). Spatio-temporal analysis of cellulose synthesis during cell plate formation in *Arabidopsis.* Plant J. **77:** 71–84.

Mim, C., Cui, H., Gawronski-Salerno, J.A., Frost, A., Lyman, E., Voth, G.A., and Unger, V.M. (2012). Structural basis of membrane bending by the N-BAR protein endophilin. Cell **149:** 137–145.

Miyagishima, S.Y., Kuwayama, H., Urushihara, H., and Nakanishi, H. (2008). Evolutionary linkage between eukaryotic cytokinesis and chloroplast division by dynamin proteins. Proc. Natl. Acad. Sci. USA **105:** 15202–15207.

Mravec, J., et al. (2011). Cell plate restricted association of DRP1A and PIN proteins is required for cell polarity establishment in *Arabidopsis.* Curr. Biol. **21:** 1055–1060.

Neumann, S., and Schmid, S.L. (2013). Dual role of BAR domain-containing proteins in regulating vesicle release catalyzed by the GTPase, dynamin-2. J. Biol. Chem. **288:** 25119–25128.

Otegui, M.S., Mastronarde, D.N., Kang, B.H., Bednarek, S.Y., and Staehelin, L.A. (2001). Three-dimensional analysis of syncytial-type cell plates during endosperm cellularization visualized by high resolution electron tomography. Plant Cell **13:** 2033–2051.

Park, E., Díaz-Moreno, S.M., Davis, D.J., Wilkop, T.E., Bulone, V., and Drakakaki, G. (2014). Endosidin 7 specifically arrests late cytokinesis and inhibits callose biosynthesis revealing distinct trafficking events during cell plate maturation. Plant Physiol. **165:** 1019–1034.

Park, M., Touihri, S., Müller, I., Mayer, U., and Jürgens, G. (2012). Sec1/Munc18 protein stabilizes fusion-competent syntaxin for membrane fusion in Arabidopsis cytokinesis. Dev. Cell **22:** 989–1000.

Park, M., Lee, D., Lee, G.J., and Hwang, I. (2005). AtRMR1 functions as a cargo receptor for protein trafficking to the protein storage vacuole. J. Cell Biol. **170:** 757–767.

Peter, B.J., Kent, H.M., Mills, I.G., Vallis, Y., Butler, P.J., Evans, P.R., and McMahon, H.T. (2004). BAR domains as sensors of membrane curvature: the amphiphysin BAR structure. Science **303:** 495–499.

Samuels, A.L., Giddings, T.H., Jr., and Staehelin, L.A. (1995). Cytokinesis in tobacco BY-2 and root tip cells: a new model of cell plate formation in higher plants. J. Cell Biol. **130:** 1345–1357.

Seguí-Simarro, J.M., Austin II, J.R., White, E.A., and Staehelin, L.A. (2004). Electron tomographic analysis of somatic cell plate formation in meristematic cells of *Arabidopsis* preserved by high-pressure freezing. Plant Cell **16:** 836–856.

Song, K., Jang, M., Kim, S.Y., Lee, G., Lee, G.J., Kim, D.H., Lee, Y., Cho, W., and Hwang, I. (2012). An A/ENTH domain-containing protein functions as an adaptor for clathrin-coated vesicles on the growing cell plate in *Arabidopsis* root cells. Plant Physiol. **159:** 1013–1025.

Stahelin, R.V., and Cho, W. (2001). Differential roles of ionic, aliphatic, and aromatic residues in membrane-protein interactions: a surface plasmon resonance study on phospholipases A2. Biochemistry **40:** 4672–4678.

Sundborger, A., Soderblom, C., Vorontsova, O., Evergren, E., Hinshaw, J.E., and Shupliakov, O. (2011). An endophilin-dynamin complex promotes budding of clathrin-coated vesicles during synaptic vesicle recycling. J. Cell Sci. **124:** 133–143.

Takei, K., Slepnev, V.I., Haucke, V., and De Camilli, P. (1999). Functional partnership between amphiphysin and dynamin in clathrin-mediated endocytosis. Nat. Cell Biol. **1:** 33–39.

Thiele, K., Wanner, G., Kindzierski, V., Jürgens, G., Mayer, U., Pachl, F., and Assaad, F.F. (2009). The timely deposition of callose is essential for cytokinesis in *Arabidopsis.* Plant J. **58:** 13–26.

Verma, D.P.S. (2001). Cytokinesis and building of the cell plate in plants. Annu. Rev. Plant Physiol. Plant Mol. Biol. **52:** 751–784.

Yin, Y., Arkhipov, A., and Schulten, K. (2009). Simulations of membrane tubulation by lattices of amphiphysin N-BAR domains. Structure **17:** 882–892.

Yoon, Y., Zhang, X., and Cho, W. (2012). Phosphatidylinositol 4,5-bisphosphate (PtdIns(4,5)P_2) specifically induces membrane penetration and deformation by Bin/amphiphysin/Rvs (BAR) domains. J. Biol. Chem. **287:** 34078–34090.

Zhang, Z., Hong, Z., and Verma, D.P.S. (2000). Phragmoplastin polymerizes into spiral coiled structures via intermolecular interaction of two self-assembly domains. J. Biol. Chem. **275:** 8779–8784.

Zhuang, X., Wang, H., Lam, S.K., Gao, C., Wang, X., Cai, Y., and Jiang, L. (2013). A BAR-domain protein SH3P2, which binds to phosphatidylinositol 3-phosphate and ATG8, regulates autophagosome formation in *Arabidopsis.* Plant Cell **25:** 4596–4615.

Zhuang, X., Cui, Y., Gao, C., and Jiang, L. (2015). Endocytic and autophagic pathways crosstalk in plants. Curr. Opin. Plant Biol. **28:** 39–47.

Zimmerberg, J., and Kozlov, M.M. (2006). How proteins produce cellular membrane curvature. Nat. Rev. Mol. Cell Biol. **7:** 9–19.